BATTERY ENERGY
Open Access

WILEY

Electrolyte engineering strategies for regulation of the Zn metal anode in aqueous Zn-ion batteries

Zixuan Li[1] | Alex W. Robertson[2]

[1]Department of Materials, University of Oxford, Oxford, UK

[2]Department of Physics, University of Warwick, Coventry, UK

Correspondence
Alex W. Robertson, Department of Physics, University of Warwick, Coventry CV4 7AL, UK.
Email: alex.w.robertson@warwick.ac.uk

Abstract

Rechargeable aqueous zinc-ion batteries (AZBs), with their high theoretical capacity, low cost, safety, and environmental friendliness, have risen as a promising candidate for next-generation energy storage. Despite the fruitful progress in cathode material research, the electrochemical performance of the AZB remains hindered by the physical and chemical instability of the Zn anode. The Zn anode suffers from dendrite growth and chemical reactions with the electrolyte, leading to efficiency decay and capacity loss. Recently, significant effort has been dedicated to regulating the Zn anode. Electrolyte manipulation, including tailoring the salt, additives, or concentration, is a useful strategy as the electrolyte strongly influences the anode's failure processes. It is thus worthwhile to gain an in-depth understanding of these electrolyte-dependent regulation mechanisms. With this in mind, this review first outlines the two main issues behind Zn anode failure, dendrite growth, and side reactions. Subsequently, an understanding of the electrolyte tailoring strategy, namely, the influence of the salt, additive, and concentration on the Zn anode, is provided. We conclude by summarizing the future prospects of the Zn metal anode and potential electrolyte-based solutions.

K E Y W O R D S

aqueous zinc-ion battery, zinc electrolyte, zinc-ion battery, zinc metal anode

1 | INTRODUCTION

The lithium-ion batteries (LIBs) have been one of the hottest subjects of electrochemical energy storage research for several decades, with intensive research in academiag1 and industry.[1–3] However, sustaining the current trend of continued iterative improvement in their energy density and cycling performance will eventually hit a fundamental limit, especially on the graphite anode side. New rechargeable battery architectures will be required. Such "beyond lithium-ion" batteries, including lithium–sulfur or lithium–oxygen, promise the realization of significantly higher energy densities.[4,5] These battery architectures are often best paired with a lithium metal anode, replacing the graphitic host anode used in current LIBs. However, lithium is reactive and unstable, leading to severe degradation issues when employed directly in its metallic state.[5] The high reactivity leads to the formation of a solid electrolyte interphase (SEI) coating across the lithium metal, due to the lithium reacting with the electrolyte. This consumes lithium, the loss of which can be cumulative over repeated cycling due to

continued SEI (re-) formation. Furthermore, irregularly shaped tortuous deposits and dendrite sections can become electrically isolated on discharge due to dissolution potentially occurring more rapidly at the deposit base, leading to detachment of the deposit from the electrode. This detached lithium is permanently unavailable for future cycling due to being fully surrounded by electrically insulating SEI and is thus known as "dead Li." The lithium dendrites may also pierce the porous separator and bring about a short circuit in the cell, causing explosions due to the organic flammable electrolyte (Figure 1A). The development of battery chemistry that is instead based around a less reactive species would allow for a metal anode that is more robust to these failure modes. Furthermore, due to the high safety demands of commercial batteries, aqueous-compatible electrolyte batteries have begun to attract attention and thus suggest a further benefit of using a less reactive metal anode chemistry. Compared to other metal anodes that are compatible with aqueous electrolytes, such as Cu and Fe, Zn metals exhibit considerable merits, including stable electrochemical activity, low cost, and environmental friendliness.[6–14] The Zn metal anode in the aqueous zinc ion battery (AZB) has a suitable equilibrium potential (−0.76 V vs. standard hydrogen electrode) and delivers a high volumetric capacity of 5855 mAh cm^{-3}.[15–22]

Nevertheless, the direct implementation of the Zn metal as a rechargeable battery anode still faces two main detrimental issues that hinder its practical application; physical and chemical instability. The former physical instability is due to Zn dendrites, caused by heterogeneous electrodeposition of Zn.[6,23–25]

Uneven electric field distribution may cause a gradual irregular accumulation of Zn over repeated charging and discharging, giving rise to the formation of Zn dendrites (Figure 1B). Typically, Zn dendrites have a two-dimensional (2D) hexagonal morphology, due to the hexagonal closed-pack structure of Zn crystals, unlike the rarefied 1D form of Li dendrites. The further growth of Zn dendrites may pierce the separator, either becoming lodged and detached within it or even resulting in a short circuit of the AZB.[26–31] Also, due to the fact that zinc dissolution can often occur at the root of Zn dendrites, the top part is likely to detach and lose electrical contact with the substrate ("dead zinc"), deteriorating the capacity of the Zn anode.[23,26,32]

The chemical instability of the Zn metal anode stems from the water molecules in the aqueous electrolyte.[28,33,34] Aqueous electrolytes have the edge over traditional organic electrolytes because aqueous electrolytes can realize higher ionic conductivity, superior kinetics at the anode–electrolyte interface, and enhanced salt solubility. In addition, it negates the formation of an electrically isolating SEI layer, which is typically formed with organic electrolytes.[1,5,35,36] However, all these advantages come with a cost. The Zn metal is thermodynamically unstable in water, leading to parasitic chemical reactions like zinc corrosion, hydrogen evolution reaction (HER), and byproduct formation (Figure 1B).[33,37] These adverse reactions keep consuming active Zn and electrolytes, hampering the cycling performance and capacity of an AZB. It is worth noting here that the physical and chemical instabilities of the Zn anode interact with each other and should not be considered independent. The formation of Zn dendrites could trigger severe side reactions, as dendrites provide
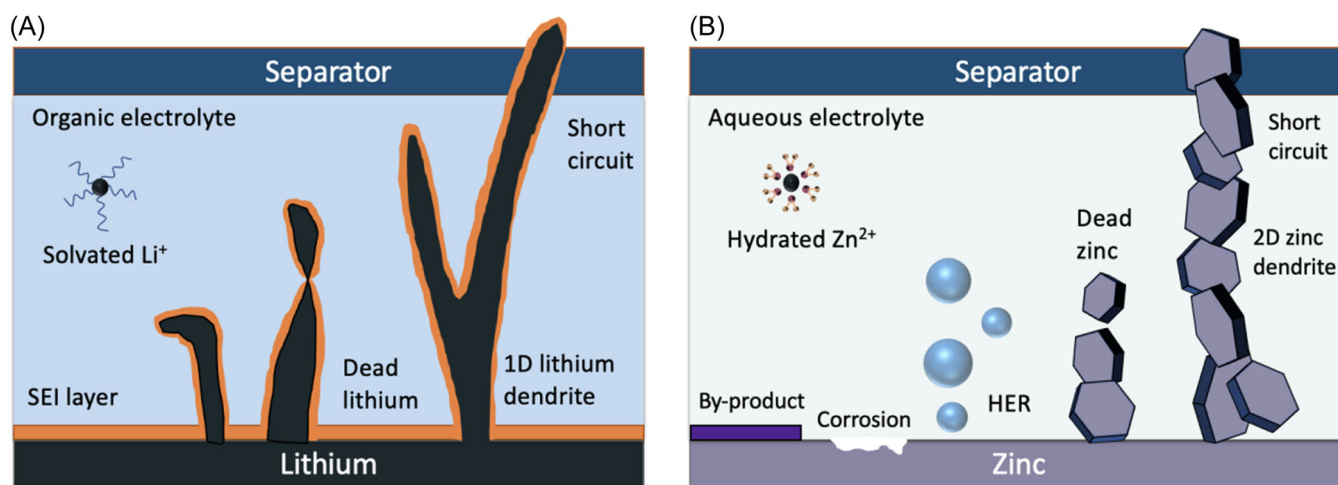

FIGURE 1 Schematic summary of degradation mechanisms for (A) an Li metal anode in an organic electrolyte and (B) a Zn metal anode in an aqueous electrolyte. HER, hydrogen evolution reaction; SEI, solid electrolyte interphase.

LI AND ROBERTSON

**BATTERY
ENERGY**
Open Access

−WILEY

3 of 30

a larger surface for active Zn to react with aqueous electrolytes. Therefore, it is worthwhile to develop regulating strategies for the Zn anode that both suppress dendrite growth and inhibit side reactions so as to achieve high-energy-density AZBs.

Ideas for suppressing Zn dendrite growth involve facilitating the Zn ion kinetics, smoothing the electric field distribution, and manipulating the Zn crystal orientation.[38–41] As for mitigating side reactions, minimizing the contact between the zinc anode and water molecules is the most direct approach.[42–45] Based on these considerations, several strategies have been proposed to tune the zinc anode, like constructing an artificial layer on the anode, designing a hierarchical 3D structure as the anode current collector, and electrolyte manipulation.[23,31,46–63] Our review explores the latter of these strategies: electrolyte engineering and tailoring to mitigate or prevent the metal anode degradation mechanisms. The electrolyte plays a pivotal role in AZBs and its intrinsic properties have multiple impacts on the performance of AZB, as the electrolyte is correlated with the electrochemical stability window, ionic conductivity, and solvation structure of Zn^{2+} ions. Manipulating the electrolyte, rather than engineering the electrode itself or introducing an artificial interface layer, can present a more elegant solution to anode degradation and benefits from being inherently more scalable to industrial applications. Altering the electrolyte composition, by introducing additives or altering the salt concentration, can be relatively easily executed and is typically straightforward to scale up. This cannot necessarily be said for artificial interfaces or designed electrodes, where the often-sophisticated nature of the structure preparation or deposition can pose additional significant challenges when considering scaling the process to industrial levels.

In this review, a systematic understanding of the Zn anode degradation issues, and potential electrolyte-based methods to regulate the Zn anode, will be discussed. The review begins with a summary of the physical and chemical instability of Zn anodes. The nucleation model and the effect of crystallographic orientation are covered in the physical Zn dendrite part. The chemical side reactions and relevant characterization methods are summarized in the Zn chemical instability part. These two parts provide the fundamental understanding for solving the issues with the Zn anode. In the following part of our review, different electrolyte engineering strategies to regulate Zn anodes are discussed. As shown in Figure 2, electrolyte engineering can suppress Zn dendrite growth through the following mechanisms: control of Zn crystallographic orientation, assembling an electrostatic shield on Zn protuberances, inhibiting Zn^{2+} ion 2D diffusion, and manipulating the Zn nucleation
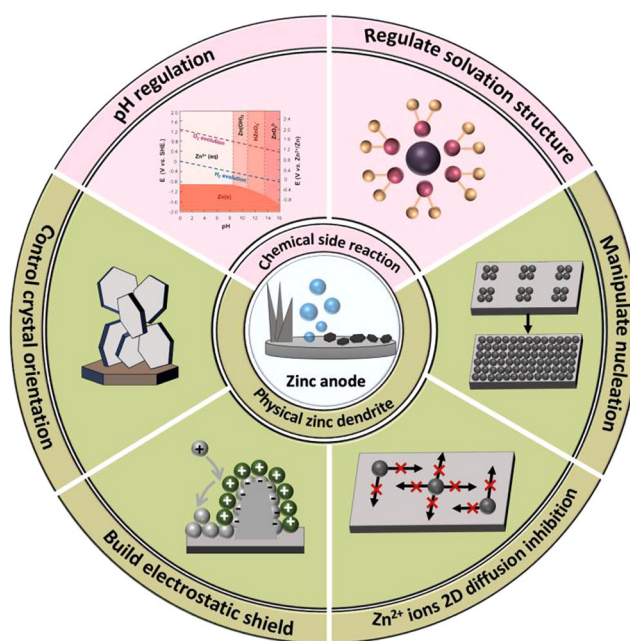

FIGURE 2 Schematic illustration of Zn anode regulation methods by tailoring the electrolyte

process. Moreover, electrolyte manipulation could mitigate chemical side reactions by regulating the pH and the Zn-ion solvation structure. This method of electrolyte engineering includes controlling salt, additive, and concentration of the electrolyte. Finally, an outlook on the mechanisms of Zn degradation and effective electrolyte design tactics have been proposed. This review is expected to provide a comprehensive strategy to regulate the Zn anode via electrolyte engineering and inspire researchers to develop electrolytes to achieve the goal of high energy density AZBs.

2 | CHALLENGES OF THE ZINC ANODE

2.1 | Physical zinc dendrite

The ideal Zn anode surface should be uniform and flat since it is beneficial for achieving high coulombic efficiency (CE) and long cycling performance. However, due to the heterogeneous electric field distribution and electrolyte concentration gradient, uneven electrodeposition of Zn is inevitable, which thus leads to Zn dendrite formation. Zn dendrites not only present the risk of puncturing the cell separator and a source of Zn loss by physical detachment but also provide more surface area for chemical side reactions. Thus, the dendrite is pivotal to battery performance, and understanding its formation mechanism is of great importance. A great amount of

effort has been spent on understanding dendrites in lithium and other battery chemistries; however, the aqueous electrolyte and lack of an SEI layer mean that the dendrite formation process is fundamentally distinct in AZBs. The formation process of zinc dendrites consists of two main parts: initial nucleation and subsequent growth.[1] Initial nucleation determines the nuclei density and the number of active nuclei sites, which has a great influence on later zinc deposition. As the reaction proceeds, further deposition on the active nucleation regions leads to Zn dendrite formation. Both initial nucleation and subsequent zinc dendrite formation mechanisms are studied in the following section.

2.1.1 | Zinc nucleation mechanism

During the initial nucleation process, there are several steps for Zn^{2+} ions in the electrolyte to become deposited as metallic zinc. An illustrative schematic diagram is shown in Figure 3A. At the pristine stage, ions are randomly distributed in the electrolyte. After applying an external current or overpotential, electric double layers are generated, namely, the inner Helmholtz layer (IHL) and the outer Helmholtz layer (OHL).[64] If the extra current is large enough, the electric double layers start to charge, and the solvated Zn^{2+} ions move from the bulk electrolyte to the electric double layers under the motivation of the electric field. When Zn^{2+} solvation sheaths pass through the IHL, they gradually desolvate and become Zn^{2+} ions. Then, Zn^{2+} ions adsorb on the surface and transfer electrons with the anode until Zn^{2+} ions are reduced to metallic Zn. The free energy curve shown in Figure 3B illustrates that Zn^{2+} ions need to overcome an energy barrier so as to reach this new phase.[73] Figure 3C shows the corresponding overpotential diagram during the Zn deposition process. The nucleation overpotential corresponds to the initial nucleation of zinc embryos, while the plateau overpotential reflects the subsequent zinc growth.[65]

Based on the classical nucleation theory, Scharifker and Hills establish a three-dimensional nucleation model with diffusion-limited growth (known as the SH
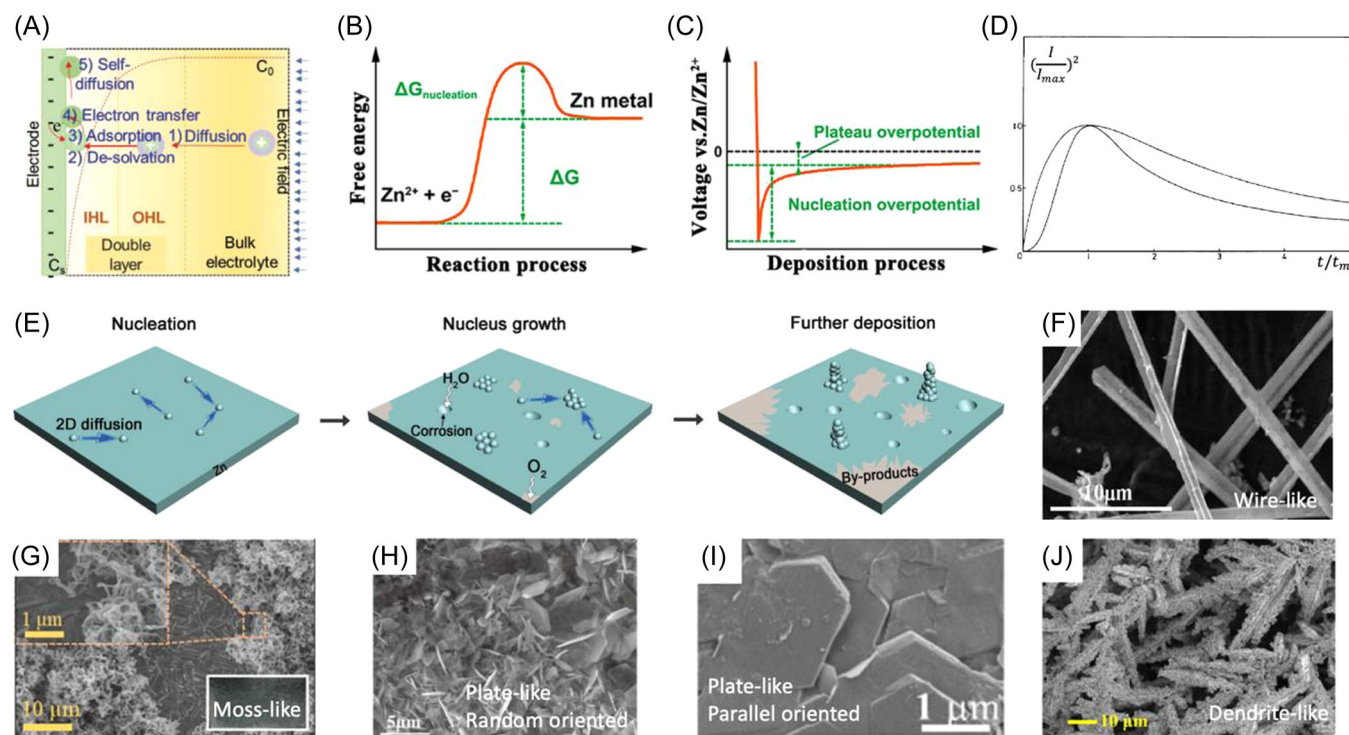

FIGURE 3 (A) Schematic of Zn^{2+} initial nucleation. Reproduced with permission, copyright 2020 Wiley.[64] (B) Changes of free energy and (C) typical voltage curve at the Zn deposition process. Reproduced with permission, copyright American Chemical Society.[65] (D) Nondimensional current transient plots for instantaneous nucleation (upper curve) and progressive nucleation (bottom curve). Modified with permission, copyright 1983 Elsevier.[66] (E) Schematic illustration of Zn dendrite growth. Reproduced with permission from the Royal Society of Chemistry.[67] Scanning electron microscopy (SEM) images of electrodeposited Zn: (F) Wire-like. Reproduced with permission, copyright IOP Publishing.[68] (G) Moss-like. Reproduced with permission, copyright American Chemical Society.[69] (H) Plate-like with random orientation. Reproduced with permission, copyright Wiley.[70] (I) Plate-like with parallel orientation. Reproduced with permission, copyright American Chemical Society.[71] (J) Plate-like with vertical orientation. Reproduced with permission, copyright American Association for the Advancement of Science.[72]

model),[66,74,75] which is the most widely used model in aqueous electrodeposition. Depending on the nucleation rate and sites, they proposed two different nucleation modes: instantaneous nucleation and progressive nucleation. Instantaneous nucleation means that nucleation occurs rapidly at a small number of active sites, whereas progressive nucleation presents nucleation occurring continually over a large number of active sites. The expressions between current transient I and deposition time t under different nucleation modes are shown below.

Instantaneous nucleation:

$$\left(\frac{I}{I_{\max}}\right)^2 = \frac{1.9542}{t/t_m}\{1 - \exp[-1.2564(t/t_m)]\}^2. \quad (1)$$

Progressive nucleation

$$\left(\frac{I}{I_{\max}}\right)^2 = \frac{1.2254}{t/t_m}\{1 - \exp[-2.3367(t/t_m)]\}^2, \quad (2)$$

where $I_{\max}$ is the maximum current transient and t_m is the corresponding time when the current reaches its maximum. The plot of the current transient under instantaneous and progressive nucleation is shown in Figure 3D.

Although the SH model has revealed new insights into the nucleation process, it can only be applied to potentiostatic electrodeposition because it uses the current density parameter to describe the equilibrium of ions in the solution and metallic phase. However, battery research generally utilizes galvanostatic cycling to study the electrochemical performance of a battery.[76–79] Also, fast-charging techniques are widely applied in industry, which means charging under galvanostatic conditions until reaching a target voltage.[79] Thus, developing a nucleation model for galvanostatic deposition is crucial, but only a few studies have attempted to explore it. Yuan et al.[80] attempt to obtain overpotential transients based on the SH model. They assume that for a certain deposition that occurs under a potentiostatic stimulus, there is a corresponding galvanostatic stimulus. It is also assumed that at the corresponding current I_0, the same mass of the metal can be deposited on the electrode with overpotential E_0. The nondimensional current plot can be transformed into the overpotential plot as Equation (3):

$$\left(\frac{I}{I_{\max}}\right)^2 = \frac{(\Delta E_0 \times I_0/\Delta E_T)^2}{(\Delta E_0 \times I_0/\Delta E_{\min})^2} = \left(\frac{\Delta E_{\min}}{\Delta E_T}\right)^2, \quad (3)$$

where ΔE_0 is the overpotential under potentiostatic stimulation, ΔE_T is the transient overpotential under galvanostatic stimulation, and $\Delta E_{\min}$ is the minimum

polarization value, which is calculated by taking the derivative of the E–t curve at zero.

Thus, for instantaneous nucleation,

$$\left(\frac{\Delta E_{\min}}{\Delta E_T}\right)^2 = \left(\frac{I}{I_{\max}}\right)^2 = \frac{1.9542}{t/t_m}$$
$$\times \{1 - \exp[-1.2564(t/t_m)]\}^2. \quad (4)$$

For progressive nucleation,

$$\left(\frac{\Delta E_{\min}}{\Delta E_T}\right)^2 = \left(\frac{I}{I_{\max}}\right)^2 = \frac{1.2254}{t/t_m}$$
$$\times \{1 - \exp[-2.3367(t/t_m)]\}^2, \quad (5)$$

where t_m is the corresponding time to the minimum polarization value.

The plot of $\left(\frac{\Delta E_{\min}}{\Delta E_T}\right)^2$ versus t/t_m shares the same trend as Figure 3D. Although Yuan et al.[80] developed a nucleation model under galvanostatic excitation, this model is not widely used, unlike the SH model that has been used in different metal deposition conditions. Furthermore, the assumptions of this model have been simplified and have not been proven to match the actual electrodeposition process. Therefore, researchers should be cautious when using this model. To sum up, in previous electrodeposition studies, people mainly focused on understanding the potentiostatic deposition, including the classical nucleation model. However, recently there has been increasing interest in understanding galvanostatic electroplating as it is the typical method for battery performance testing. Unfortunately, to date, there is no comprehensive nucleation model that has been widely used and verified as suitable for galvanostatic electrodeposition. Thus, more attention needs to be paid to establishing models to describe galvanostatic deposition.

2.1.2 | Zinc dendrite formation

Figure 3E shows the mechanism of zinc dendrite formation. At the initial nucleation stage, Zn^{2+} ions prefer to nucleate at tips, grain boundaries, impurities, and dislocations. During the following electrodeposition processes, the zinc crystals are not uniformly deposited on the substrate, but mainly on the previous nucleation sites. This can be attributed to the resulting uneven distribution of the electric field and the gradient of the electrolyte concentration. Due to the uneven anode surface, the electric field strength at the tip is higher

than elsewhere, causing Zn^{2+} ions to deposit at the tip.[64,81,82] These tips can further induce the accumulation of more zinc electrodeposits on them, leading to the growth of zinc dendrites.[31,67] As these dendrites may puncture the separator and cause detached "dead zinc," which is detrimental to battery capacity and life span, a flat Zn anode is desired as it can induce uniform plating and prevent Zn dendrites. This understanding has been exploited in recent literature, with zincophilic host electrode materials used as an effective dendrite prevention strategy. Zn^{2+} ions are inclined to bond with zincophilic sites like N-doping graphene, Ag, Cu, Sn, TiO_2, and ZIF-8.[83–89] The zincophilic sites reduce the nucleation barrier of Zn^{2+} ions and enhance the interaction with Zn^{2+} and the anode host, thus preventing aggregated Zn nucleation and ensuring homogeneous deposition of Zn.

We can use two parameters to describe the morphology of Zn deposits: (i) the shape of individual zinc particles and (ii) the way the zinc particles are oriented on the anode. Some typical scanning electronic microscopy (SEM) images of electrodeposited Zn are shown in Figure 3F–J. In the aqueous electrolyte, individual zinc deposits can be wire-like (Figure 3F), mossy-like (Figure 3G), and plate-like (Figure 3H–J). In the commonly used mildly acidic zinc electrolyte, it tends to be plate-like because the hexagonal closed-packed Zn crystals prefer to expose the (002) plane to minimize the migration energy. The orientation of Zn plates can be random (Figure 3H), parallel (Figure 3I), and vertical (Figure 3J). Section 2.1.3 will cover Zn crystal orientation in detail.

2.1.3 | Crystallographic orientation

Since zinc is a crystalline metal, its anode surface texture can be altered by controlling its crystallographic orientation. When zinc ions nucleate in the first stage of electrodeposition, they nucleate randomly in different orientations. As the reaction continues, zinc crystals tend to grow through the (001) facet due to the hexagonal close-packed structure of zinc, thus generating hexagonal plates in different directions. If the zinc plates grow vertically on the surface, it is easier for small zinc plates to grow during the charge–discharge process and then forms zinc dendrites. However, if zinc plates grow parallel to the anode surface, a uniform and flat surface can be achieved. The anode current collector substrate can determine whether the zinc is deposited epitaxially or nonepitaxially, as shown in Figure 4A. Epitaxial deposition (right part in Figure 4A) is ideal because, by choosing the right substrate, it locks the zinc metal to

grow in specific directions, whereas nonepitaxial (left part in Figure 4A) deposition means that zinc crystals may form in random directions. Generally, if the atomic radius of the substrate is similar to that of the zinc basal plane (lattice mismatch is less than 15%), the zinc crystal will tend to grow parallel to the substrate.[90,92,93]

Taking advantage of this property, Zheng et al.[90] proposed to deposit zinc on graphene, deposited so that it has more 001 phase exposure. The lattice difference between $(001)_{graphene}$ and $(002)_{Zn}$ is 7%, which can lead to the parallel growth of zinc. Thus, epitaxially grown Zn improves the CE (99.9%) for 1000 cycles at a high current density of $4\,mA\,cm^{-2}$, comparing favorably to a pure polycrystalline Zn anode. This work well illustrates how dendrite-free zinc anodes can be achieved by developing a uniform zinc surface by tuning the anode substrate. Other substrates, which can also induce Zn crystal parallel growth, have been reported, including chemical vapor deposition (CVD)-grown graphene, Sn-textured surface, (100)-dominated Cu current collector, and rolled (002)-exposed Zn foil.[69,70,94,95] However, these slight lattice-mismatched substrates cannot completely prevent the vertical growth of zinc. When the two deposited zinc islands meet each other, the small lattice mismatch between the zinc and the substrate will prevent the two islands from merging together. This may lead to the formation of zinc dendrites at the interface of the two islands, as shown in Figure 4B. Pu et al.[91] claimed to develop perfect lattice-matched zinc deposition by using a single-crystal zinc anode (Figure 4C–E). Since zinc is deposited directly on the zinc substrate (homoepitaxial growth), rather than a foreign substrate, the energy barrier to overcome by zinc ions is relatively low. Figure 4F–H shows that discrete zinc islands merged to form a larger single grain, rather than imperfect polycrystalline stitching, and thus a uniform Zn surface could be maintained.

2.1.4 | External factors affecting zinc dendrite

Current density: The current density has a great influence on the dendrite formation rate and Zn crystal orientation.[6,30,65,96–102] According to the kinetic diffusion-limited model, zinc ion concentration near the electrode surface is determined by the current density. High current density leads to rapid electrolyte depletion near the anode surface, causing a large concentration gradient between the reaction zone and the bulk electrolyte.[27,103,104] Due to local deviations Zn dendrites are thus likely to form. However, opposing views have been raised on the ease of forming dendrites at high current densities. Hou et al.[105]
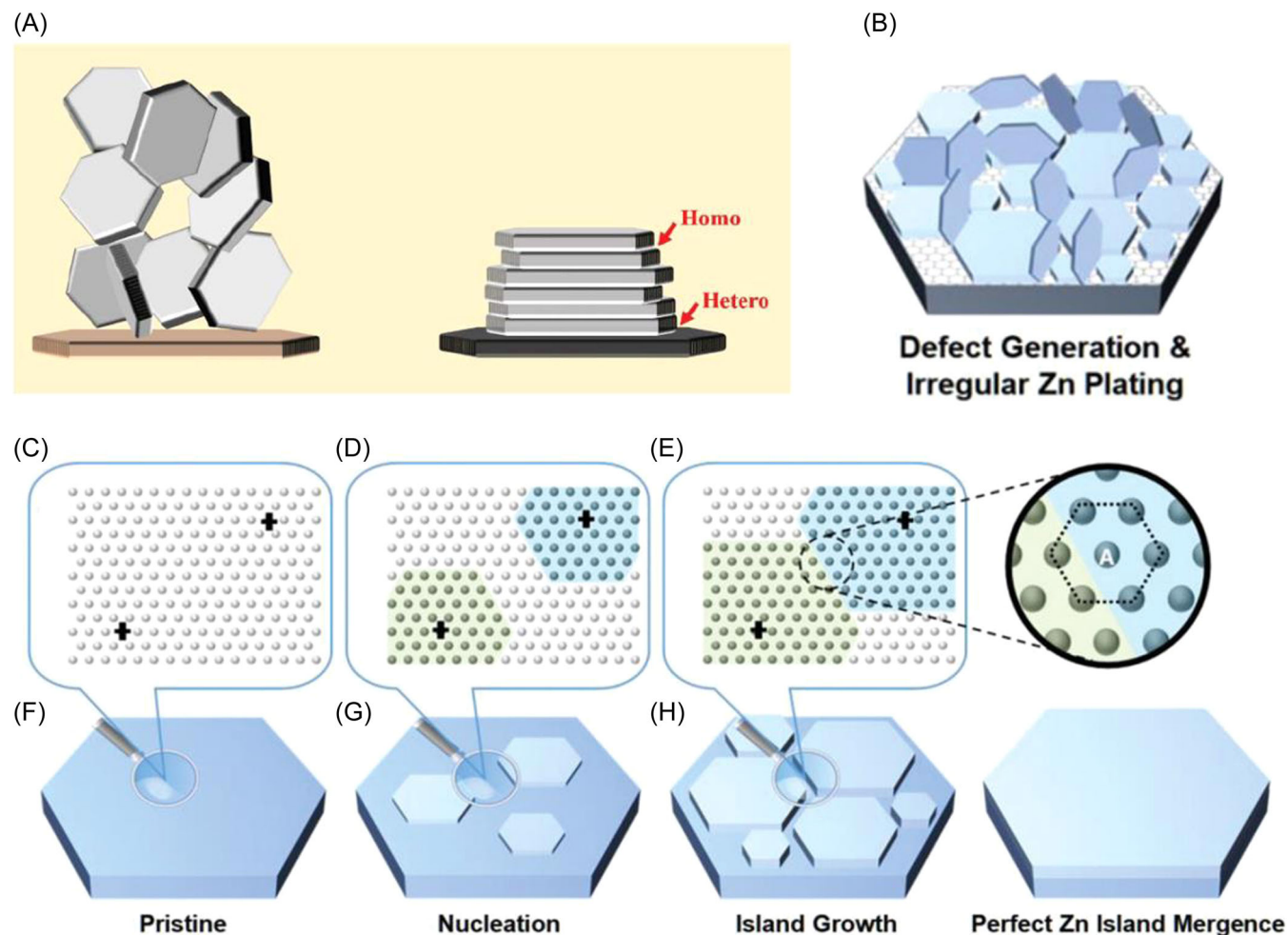
FIGURE 4 (A) Schematic of epitaxial and nonepitaxial zinc deposition. Reproduced with permission, copyright American Association for the Advancement of Science.[90] (B) Schematic of electrodepositing Zn on the small lattice-mismatched substrate. Schematic of electrodepositing Zn on the perfect lattice-matched substrate: (C–E) Zn atomic arrangements and interisland stitching and (F–H) morphology change of the Zn anode. Reproduced with permission, copyright Wiley.[91]

argue that in addition to kinetics, thermodynamics is another element to affect zinc morphology. The Gibbs free energy of forming nuclei with radius r comprises a surface-free energy and a bulk energy. Based on classical homogeneous nucleation, the critical radius of spherical nuclei is $r = 2\gamma V_{\mathrm{m}}/F\eta$, which means radius r is inversely proportional to the overpotential η. In other words, the size of zinc particles decreases with the rise in overpotential η. Liu et al.[106] galvanized stainless steel with current densities ranging from 0.25 to 20 mA cm^{-2}. Figure 5A displays the size distribution of the corresponding zinc flakes. It is clear that both the size and distribution reduce with increasing current density. Moreover, the nuclei density of zinc flakes increases concomitantly with the current.[106] The schematic of deposited zinc flakes varying with current density is shown in Figure 5B. Since there are more zinc embryos and smaller zinc flakes generating at a high current density, the zinc surface will overall be more uniform and not generate more severe perturbations that can encourage dendrite growth.[106] In addition, the current density of zinc deposition also affects the crystal orientation.[99] It is evident in SEM images from Figure 5C–H that at low current density (1 mA cm^{-2}), zinc randomly orients on the electrode. The deposited zinc at a high current density of 20 mA cm^{-2} shows a different morphology, with a preferred orientation and a more denser texturing.[102,107] Although high current density can improve nuclei density and decrease the particle size from a thermodynamic point of view, it does not mean that ultrahigh current density is desired because it could cause kinetic instability. It is conjectured that a high current density is a double-edged sword, thus a balance should be achieved between the thermodynamic and kinetic considerations.[105]

Temperature: An external factor, temperature, can directly influence the deposition of zinc through texture
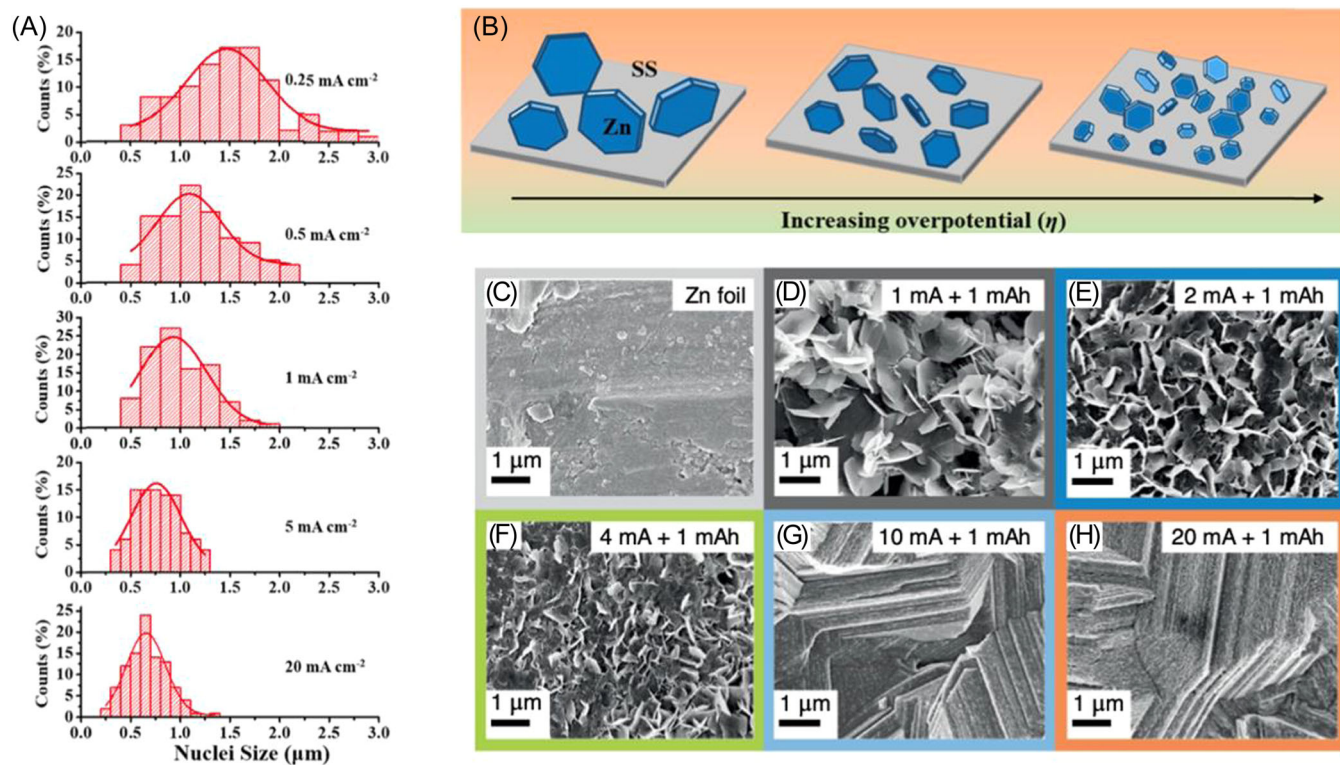
FIGURE 5 (A) Size distribution of Zn flakes when depositing from 0.25 to 20 mA cm^{-2}. (B) Schematic illustration of Zn nuclei with increasing overpotential. Reproduced with permission, copyright American Chemical Society.[106] Scanning electron microscope images of the cycled Zn electrode in a 3 M ZnSO$_4$ electrolyte: (A) Pristine Zn foil and the Zn foil anodes after cycling at (B) 1 mA cm^{-2}, (C) 2 mA cm^{-2}, (D) 4 mA cm^{-2}, (E) 10 mA cm^{-2}, and (F) 20 mA cm^{-2} at 1 mAh cm^{-2}. Reproduced with permission, copyright American Chemical Society.[107]

behavior and nucleation performance.[108–111] As the temperature increases, the conductivity and ionic association of the electrolyte also increase, resulting in faster movement of zinc ions and lower initial nucleation potential. In other words, zinc ions tend to nucleate and self-diffuse at high temperatures. Su et al.[110] investigated Zn deposits in 2 M ZnSO$_4$ at temperatures from 10°C to 60°C. The morphology and size distribution can be seen in Figure 6A–F. As the deposition temperature increases from 10°C to 60°C, the size of zinc flakes grew dramatically, and the nuclei density of Zn deposition decreased from 0.64 to 0.003 μm^{-2}. Figure 6G shows a schematic that illustrates the zinc deposition mechanism at different temperatures. Large zinc flake size and low nuclei density have been observed at a high working temperature, which can be ascribed to the fast movement and diffusion of zinc ions. In contrast, at a low temperature, the sluggish motion of zinc ions in the electrolyte leads to dense and homogeneous deposition of zinc and preferred orientation. Based on this result, they proposed a self-healing idea to prolong the cycling performance of a battery.[110] The idea is to eliminate Zn dendrites, which built up at high temperatures by self-healing them at low temperatures. The Zn//Zn symmetrical battery can only maintain 23 h of cycling at 60°C due to dendrite formation. But after subsequently cycling this battery at 25°C for 40 h, the zinc dendrites can be eliminated. Because dendrites are eliminated at relatively low temperatures, the battery can be recirculated at 60°C for 94 h, as shown in Figure 6H. Thus, the relatively low temperature can facilitate the smooth and flat deposition of zinc on the anode, thereby extending the lifespan of zinc-ion batteries.

2.2 | Chemical side reaction

2.2.1 | pH influence

Chemical side reactions occur between the Zn anode and electrolyte, thus the pH of the electrolyte determines the type of side reaction.[8,112] Figure 7A displays the Pourbaix diagram of zinc (the plot of the equilibrium potential of electrochemical reactions by the function of pH).[116] It shows that in an alkaline electrolyte, Zn will be oxidized to ZnO. The specific reaction is that due to a large amount of OH$^-$ in the electrolyte, the Zn metal would coordinate with OH$^-$ to form zincate complex Zn
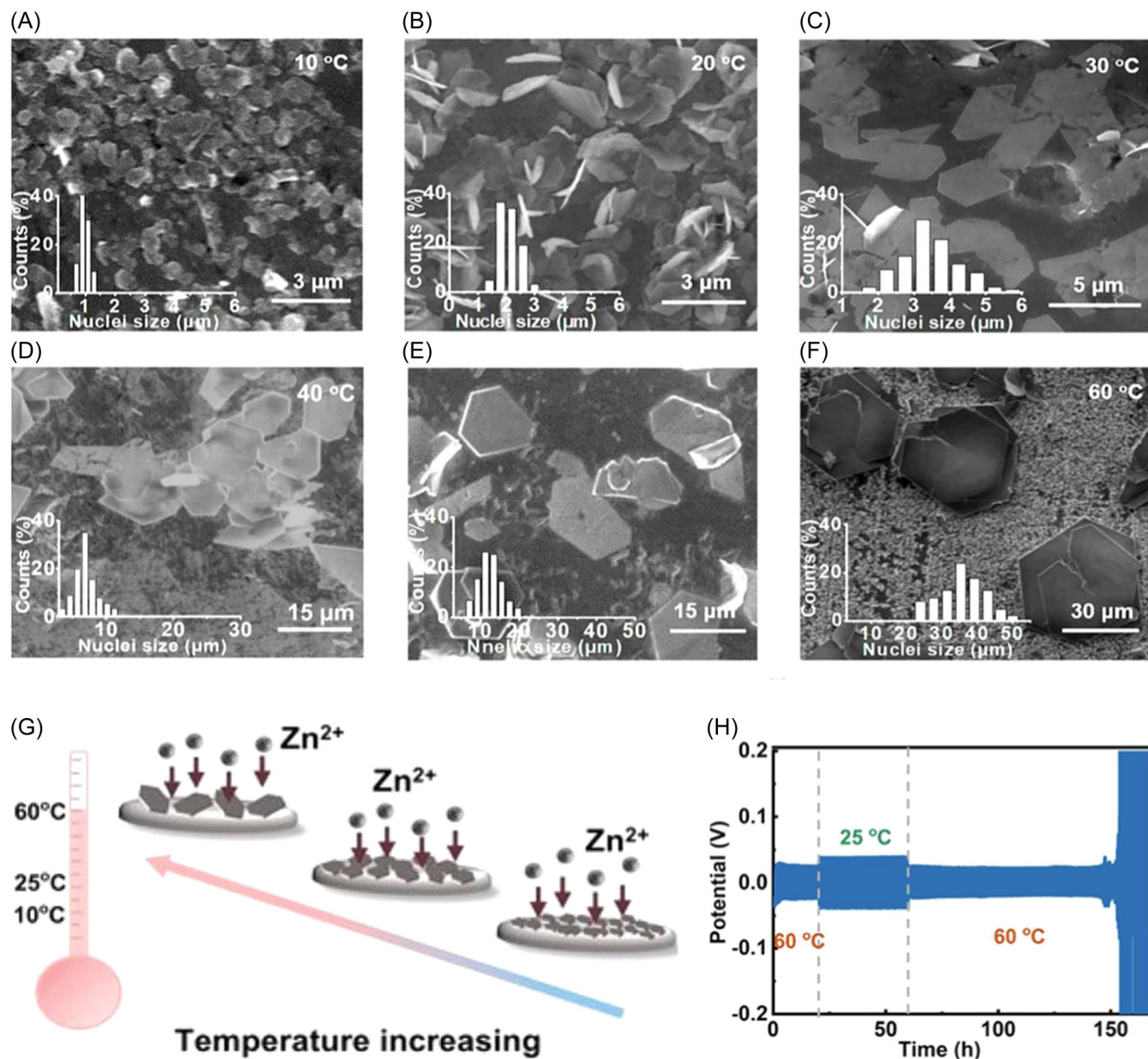
FIGURE 6 Scanning electron microsope images of the Zn deposited on the Ti substrate at different temperatures: (A) 10°C, (B) 20°C, (C) 30°C, (D) 40°C, (E) 50°C, and (F) 60°C. The capacity is $0.25\,\text{mAh}\,\text{cm}^{-2}$ and the current density is $0.5\,\text{mA}\,\text{cm}^{-2}$. (G) Schematic illustrating deposited Zn anode morphology change with increasing temperature. (H) Voltage profile of Zn//Zn symmetric cells cycled at 60–25–60°C. The capacity is $0.25\,\text{mAh}\,\text{cm}^{-2}$ and the current density is $0.5\,\text{mA}\,\text{cm}^{-2}$. Reproduced with permission, copyright American Chemical Society.[110]

$(OH)_4^{2-}$. When $Zn(OH)_4^{2-}$ reaches its saturation limit, it would subsequently dehydrate and form precipitate ZnO.[28,117] The reaction equation is as follows:

$$Zn(s) + 4OH^- \leftrightarrow Zn(OH)_4^{2-}(aq) + 2e^-,$$

$$Zn(OH)_4^{2-} \leftrightarrow ZnO(s) + H_2O + 2OH^-.$$
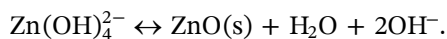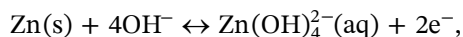
Since ZnO is insoluble in the electrolyte, this solid–liquid–solid reaction $[Zn(s)–Zn(OH)_4^{2-}(aq)–ZnO(s)]$ is not completely reversible. Thus, most of the Zn could gradually be oxidized to ZnO over repeated charging/discharging, leading to low CE and bad cycling performance.

Due to the performance problems of alkaline electrolytes in rechargeable AZBs, weakly acidic zinc electrolytes are drawing more attention in recent years. In an alkaline electrolyte, the dominant charge carrier is $Zn(OH)_4^{2-}$, while in a weakly acidic electrolyte, Zn^{2+} is the dominant carrier.[118] As shown in the following

reaction, the reaction is reversible, indicating better CE and faster Zn^{2+} kinetics.

$$Zn \leftrightarrow Zn^{2+} + 2e^-.$$
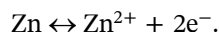
Thus, the pH of the electrolyte can strongly influence the reversibility of the Zn anode.

2.2.2 | Zn corrosion

For aqueous secondary zinc metal anode batteries, many recent studies have focused on electrolytes that are mildly acidic, with a pH of around 3–5. Although the acidic electrolyte has many advantages, it still has the problem of corroding the Zn anode. A Zn anode is thermodynamically unstable in contact with mildly acidic electrolytes. As shown in Figure 7A, the standard reduction potential of Zn/Zn^{2+} is lower than the equilibrium potential of H/H_2 in the whole pH region. Zinc corrosion and the hydrogen evolution reaction occur simultaneously. Zn(s) will be oxidized to Zn^{2+}(aq) in the mildly acidic electrolyte and H^+ in the electrolyte will be reduced to H_2. The redox reaction

leads to continuing zinc corrosion that not only consumes active zinc but also increases the interface resistance.

2.2.3 | Hydrogen evolution reaction

As mentioned, the hydrogen evolution reaction (HER) happens simultaneously with the chemical corrosion of the metallic zinc anode. Its reaction equation is as follows:

$$2H^+ + 2e^- \rightarrow H_2$$

H_2 evolution is a nonnegligible problem because it gradually consumes H^+ in the electrolyte. In addition, in sealed zinc battery systems, gas can impede the connection of the electrolyte to the electrode, thereby increasing the internal resistance of the battery and resulting in low CE. Moreover, too much gas can swell the battery and even cause it to explode. The actual HER is related to the surface of the zinc anode and the anode–electrolyte interface, with the formation of zinc dendrites increasing the surface area of the zinc anode, thus providing more area for zinc corrosion and hydrogen evolution.
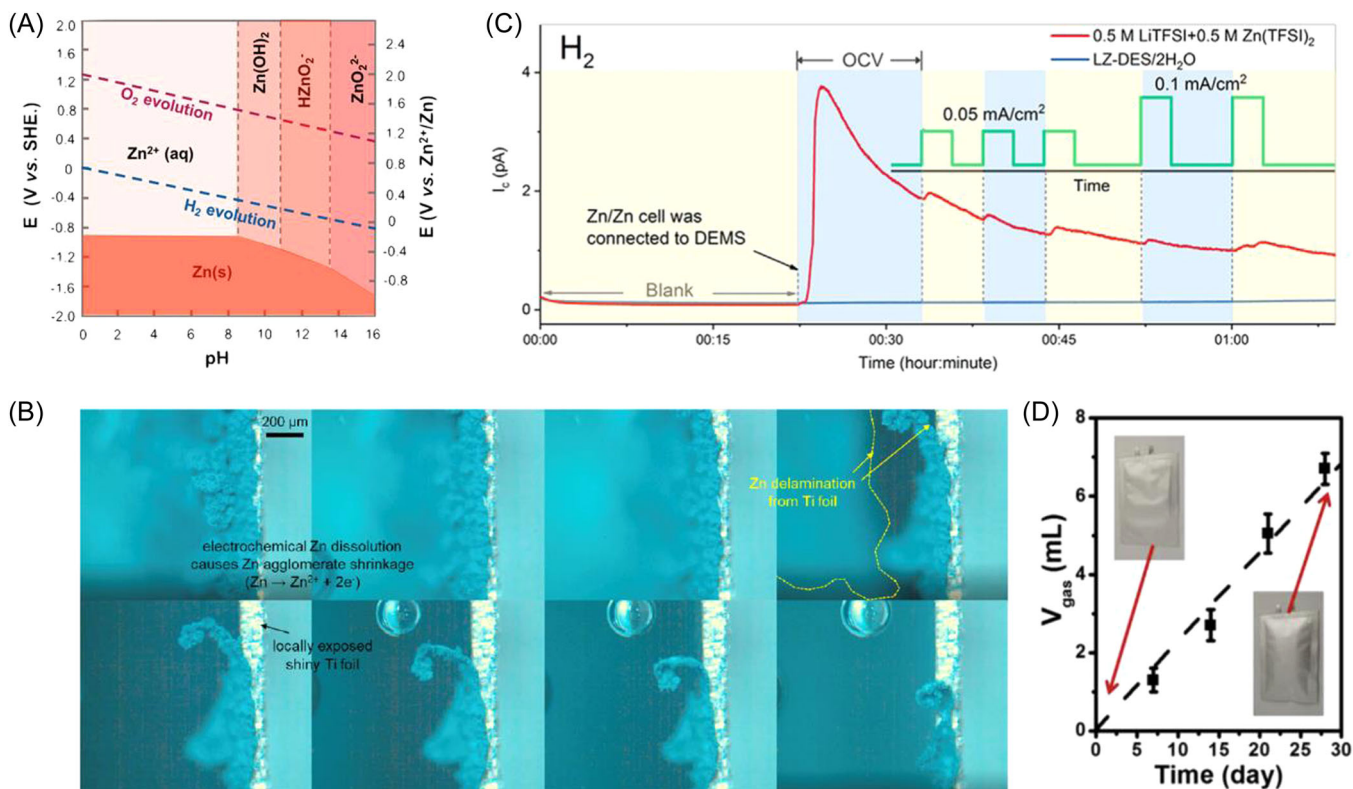

FIGURE 7 (A) Pourbaix diagram of the Zn/H_2O system with H_2 and O_2 evolution overpotential. Reproduced with permission, copyright American Chemical Society.[113] (B) Operando optical microscopy result of the Zn stripping process on Ti foil in 1 M $ZnSO_4$. Reproduced with permission, copyright Elsevier.[114] (C) Differential electrochemical mass spectrometry result for Zn//Zn cells in 0.5 M $LiTFSI + 0.5$ M $Zn(TFSI)_2$ and $LZ-DES/2H_2O$ electrolytes. Reproduced with permission, copyright Elsevier.[63] (D) Volume of hydrogen evolution in 3 M $ZnSO_4$ for different aging times. Reproduced with permission, copyright Elsevier.[115]

To detect bubbles of H_2, in situ optical microscopy is particularly helpful. Lee et al.[114] studied zinc plating and stripping behavior in a home-made cell (Figure 7B). They found that during stripping, deposited Zn gradually detached from the Ti electrode, exposing a bare shiny Ti substrate. In the meantime, hydrogen bubbles are generated at the interface with exposed Ti and delaminated Zn, and these bubbles further accelerated the detachment process of Zn. The bubble remained when zinc was stripped back into the electrolyte. Differential electrochemical mass spectrometry (DEMS) is also a useful tool to quantify the gas formation and has been widely utilized in lithium-ion battery studies. Zhao et al.[63] found that H_2 is formed even at an open-circuit voltage, which implies that the HER occurs immediately after the zinc anode comes in contact with the weakly acidic electrolyte (Figure 7C). As can be seen from the mass spectrometry trace, when a Zn//Zn symmetrical cell is cycled at 0.05 and 0.1 mA cm^{-2}, the signal peak of H_2 exists during the whole process. It suggests that the HER occurs throughout the life of the battery. Cai et al.[115] quantified the exact volume of electrochemically formed H_2 in the pouch cell setup. As shown in Figure 7D, ~6.7 ml of H_2 gas was generated after the cell was aged for 28 days, while ~19.8 μl of the electrolyte was consumed, correspondingly oxidizing ~15.9 mAh of Zn.

2.2.4 | Side product formation

In the weakly acidic electrolyte, during the hydrogen evolution reaction, the continuous consumption of H^+ leads to a local increase in pH near the electrode surface due to the accumulation of OH^-. OH^- reacts with Zn^{2+} and cations in the electrolyte to form insulating byproducts that could weaken the electrochemical performance of the battery.[53,119,120] When zinc is deposited in an alkaline electrolyte (pH around 9), the products are ZnO and Zn$(OH)_2$. However, for weakly acidic electrolytes, the product remains inconclusive. In recent studies, ZnO, Zn$(OH)_2$, and zinc hydrated sulfate (ZHS) have been reported as byproducts; Cai et al.[115] found that $Zn_4(OH)_6SO_4 \cdot xH_2O$ is generated on the zinc anode from $ZnSO_4$, which is supported by X-ray diffraction (XRD) results. The general reaction can be expressed as

$$4Zn^{2+} + 6OH^- + SO_4^{2-} + xH_2O \leftrightarrow Zn_4SO_4$$
$$(OH)_6 \cdot xH_2O.$$
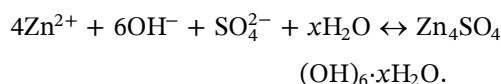
The SEM image in Figure 8A shows that the surface of pristine zinc foil was smooth, and after immersion in $ZnSO_4$ solution for 30 days, some flakes were formed on
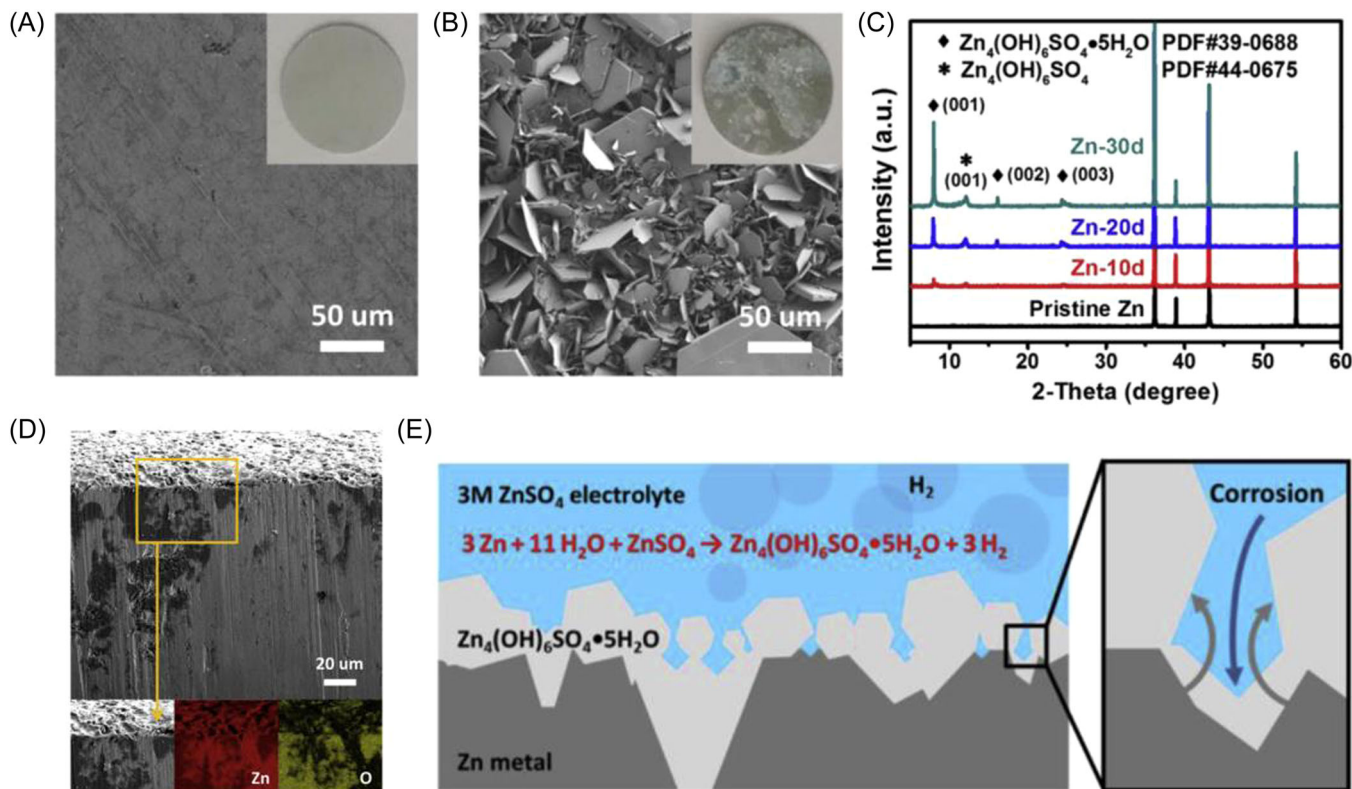

FIGURE 8 Scanning electron microscope (SEM) images of (A) pristine Zn anode and (B) Zn anode soaked in the electrolyte for 30 days. (C) X-ray diffraction result of Zn foil with different corrosion times. (D) Cross-section SEM image and energy-dispersive spectroscopy mapping of aged Zn foil. (E) Schematic of the side product formation process. Reproduced with permission, copyright Elsevier.[115]

the zinc foil (Figure 8B). These flakes have been verified as $Zn_4(OH)_6SO_4 \cdot xH_2O$ by their XRD pattern, as shown in Figure 8C. The cross-section SEM image and energy-dispersive spectroscopy mapping in Figure 8D depict that the deepest corrosion point can reach 132.2 μm. The schematic in Figure 8E illustrates that the corrosion reaction did not stop due to the loose structure of the byproduct.[115] Similar byproducts were reported in other zinc electrolytes $(Zn(CF_3SO_3)_a(OH)_b \cdot xH_2O$ in $Zn(CF_3SO_3)_2$,[121] $Zn_4ClO_4(OH)_7$ in $Zn(ClO_4)_2$.[121,122] With the combination of solvent decomposition and zinc complexation, $Zn_{12}(SO_4)_3Cl_3(OH)_{15} \cdot 5H_2O$ was reported in the $ZnCl_2$–H_2O–DMSO electrolyte.[51] Unlike the relatively dense SEI layer that forms in LIBs, coating and effectively "passivating" the entire electrode, by-products in AZB are in the form of loose flakes that do not prevent active zinc from contacting the electrolyte, allowing for continued corrosion to occur.[115] In addition, since the byproducts are hydrated, there is less water in the electrolyte, which may cause zinc salt to reach the saturation level and then precipitate due to the lack of solvent. The insulating byproduct layer could also increase the interface resistance between the zinc anode and electrolyte, thereby slowing zinc ion migration.

3 | MANIPULATING THE ZINC ELECTROLYTE TO REGULATE THE ZN ANODE

3.1 | Salts

In the zinc electrolyte, the anion of the salt determines the electrolyte properties, including the ionic conductivity, ion transfer number, and viscosity. In some salts, anions participate in the zinc solvation structure, which is a key factor affecting the zinc electrodeposition process and zinc texturing behavior at the anode. Thus, choosing suitable salts for the electrolyte may help address issues regarding zinc dendrite growth and parasitic reactions. Currently, many inorganic ($ZnCl_2$, $Zn(NO_3)_2$, $Zn(ClO_4)_2$, ZnF_2, ZnI_2, $ZnSO_4$, $ZnBr_2$) and organic ($Zn(CH_3COO)_2$, $Zn(CF_3SO_3)_2$ [also written as $Zn(OTf)_2$], zinc bis(trifluoromethanesulfonyl) [could be written as $Zn(TFSI)_2$], $Zn(CH_3CH_2SO_3)_2$, $Zn(CH_3SO_3)_2$) salts have been reported in aqueous zinc electrolytes.[107,123–132] A summary of different salts is shown in Table 1.

In the recent literature, $ZnSO_4$ is the most widely used salt due to its inherent merits of high ionic conductivity, good solubility, and excellent compatibility with cathode materials. However, when the Zn metal is in contact with $ZnSO_4$, byproducts such as ZHS are formed on the surface of the zinc anode, which hinders its electrochemical performance.

Alternative anions like NO_3^- have a high oxidizing ability, which can oxidize the zinc anode and lead to serious zinc corrosion.[133,134] Since OH^- accumulates during operation, local pH will increase, possibly involving the entire electrolyte. The Zn//copper hexacyanoferrate full cell with the $Zn(NO_3)_2$ electrolyte can only maintain 21% capacity after 200 cycles. This can be ascribed to the loss of active Zn, which has been oxidized to ZnO and $Zn(OH)_2$ due to the high oxidant NO_3^-.

Generally, $ZnCl_2$ has a low solubility in water, which means that it is difficult to achieve high concentrations of $ZnCl_2$ without adjusting pH. Furthermore, its narrow potential window (-0.1 to 0.15 V vs. Zn^{2+}/Zn) and large polarization at high voltage (over 0.6 V) limit the application of $ZnCl_2$ in Zn-ion batteries,[126] as shown in Figure 9A. In addition, other zinc halides like ZnF_2, ZnI_2,

TABLE 1 Summary of different Zn salts for AZB electrolytes

Salt	Advantages	Disadvantages
$ZnSO_4$	High ionic conductivity; good solubility; excellent compatibility with cathode materials	Side product formation
$ZnNO_3$	Low cost	High oxidizing ability
$ZnCl_2$	Low cost	Low solubility; narrow potential window; large polarization at high voltage
ZnF_2, ZnI_2, $ZnBr_2$	Minor side reaction	Low solubility
$Zn(CH_3COO)_2$	Low cost; environmentally friendly	Side product formation
$Zn(ClO_4)_2$	Good cycling performance	Potential safety hazard
$Zn(CF_3SO_3)_2$	Weaken solvation effect; control Zn orientation	High cost
$Zn(TFSI)_2$	Weaken solvation effect	High cost

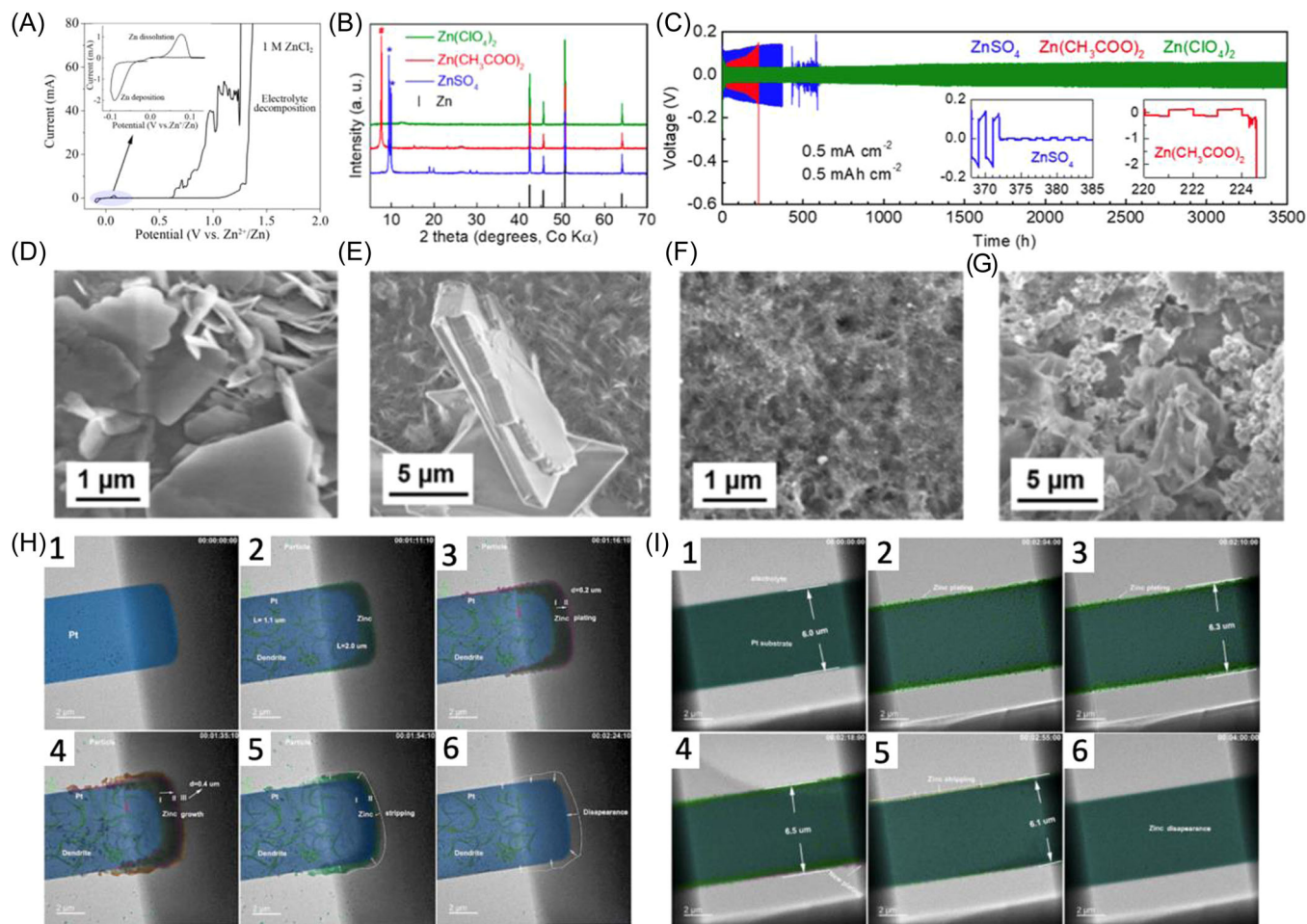Abbreviation: AZB, aqueous zinc-ion battery.

FIGURE 9 (A) Cyclic voltammograms of the Zn anode in 1 M ZnCl₂. Reproduced with permission, copyright American Chemical Society.[126] (B) X-ray diffraction patterns of Zn anodes after 50 cycles in 1 M ZnSO₄, Zn(CH₃COO)₂, and Zn(ClO₄)₂ electrolytes. (C) Cycling performance of Zn symmetric cells with a current density of 0.5 mA cm⁻² and a capacity of 0.5 mA cm⁻². Scanning electron microscope (SEM) images of the Zn anode after (D) one deposition and (E) 50 cycles in 1 M ZnSO₄. SEM images of the Zn anode after (F) one deposition and (G) 50 cycles in 1 M Zn(ClO₄)₂. (B)–(G) Reproduced with permission, copyright American Chemical Society.[125] In situ liquid cell transmission electron microscope imaging: Zn plating/stripping process in (H) 20 mM ZnSO₄ and (I) 20 mM of Zn(CF₃SO₃)₂. Zn plating is from 1 to 3 and Zn stripping is from 4 to 6. Reproduced with permission, copyright American Chemical Society.[124]

and ZnBr₂ all face the same problem of low solubility. Although these zinc halides have only minor side reactions with the zinc anode due to their low oxidative anions, it is still difficult to apply them in practical zinc electrolytes.

Zn(CH₃COO)₂ is environmentally friendly and cheap; however, it suffers from serious side reactions. In the XRD pattern of the Zn electrode cycled in Zn(CH₃COO)₂ for 50 times (Figure 9B), in addition to the Zn signal, there are several peaks of carboxyl-containing byproducts, illustrating serious side reactions during the cycling process.[125]

The selection of zinc salt can inhibit zinc dendrite formation to some extent. Wang et al.[125] found that, compared with ZnSO₄ and Zn(CH₃COO)₂, a Zn//Zn symmetrical cell with a Zn(ClO₄)₂ electrolyte can

maintain a longer cycling time to 3500 h (0.5 mA cm⁻², 0.5 mAh cm⁻²), showing better cycling performance (Figure 9C). This can be attributed to the morphology of zinc electrodeposition in different electrolytes. As is shown in Figure 9D,E, the zinc electrode after the first deposition from the ZnSO₄ electrolyte exhibits a platelet morphology. These platelets grow larger over cycling. However, zinc anodes deposited and cycled 50 times from Zn(ClO₄)₂ exhibit uniform coverage (Figure 9F,G), without any obvious zinc dendrites. This work demonstrates that using a Zn(ClO₄)₂ salt can facilitate stable zinc plating/stripping.

Zn(CF₃SO₃)₂, with its bulky anion CF₃SO₃⁻, has been reported to suppress dendrites as well.[107,124] The dynamic behavior of zinc depositing/stripping from Zn(CF₃SO₃)₂ has been revealed by an operando liquid

cell transmission electronic microscopy (TEM) study.[124] For comparison, they performed experiments with the $ZnSO_4$ electrolyte first. Figure 9H displays that with $ZnSO_4$, a dense zinc layer formed at the tip, and zinc dendrites are generated at the body during the initial deposition process. However, these zinc deposits cannot be completely removed during subsequent stripping, indicating the low CE of $ZnSO_4$. Furthermore, the Zn stripping rate is slightly lower than the deposition rate, which can be attributed to insulating byproduct formation and potentially the hydrogen evolution reaction. However, uniformly deposited zinc was found in $Zn(CF_3SO_3)_2$ with dendrite-free morphology, which is shown in Figure 9I. During the Zn stripping process, all the deposited zinc can be dissolved, showing accelerated kinetics of zinc stripping/plating. The better performance of $Zn(CF_3SO_3)_2$ is owed to the bulky anion $CF_3SO_3^-$, which has the ability to reduce the number of water molecules around the solvated Zn^{2+} ions. Less water in the Zn^{2+} solvation structure mitigates the solvation effect and accelerates the migration of Zn^{2+}. $Zn(TFSI)_2$ with its bulky anion $TFSI^-$ has also been reported as a promising electrolyte to achieve excellent reversibility in AZB.

Moreover, the electrolyte salt can tune the crystallographic orientation of the deposited Zn structure. Yuan et al.[135] demonstrated that sulfonate (SO_3^-)-based electrolytes can induce the growth of $(002)_{Zn}$ planes as the sulfonate group is able to rebuild the octahedral coordination geometry of the Zn^{2+} ion at the anode–electrolyte interface. Figure 10A shows the process of $(002)_{Zn}$ planar growth promoted by sulfonate (SO_3^-)-based anions. As is shown in Figure 10B, the metallic zinc obtained by deposition in $Zn(CF_3SO_3)_2$ has a preferred (002) orientation, while the zinc electrodeposited in $ZnSO_4$ shows more exposed (101) planes and random orientation. The SEM image in Figure 10C also confirms hexagonal-like plates stacking on the surface. Density function theory (DFT) was performed to understand the superior performance of the sulfonate group. In $Zn(CF_3SO_3)_2$, two $CF_3SO_3^-$ anions could replace two water molecules in the Zn^{2+} solvation structure $(Zn(H_2O)_6^{2+})$ and form a new solvation structure $(Zn(CF_3SO_3)_2(H_2O)_4)$. In this new solvation structure, the Zn–O bond length between Zn^{2+} and $CF_3SO_3^-$ is shorter than that between Zn^{2+} and H_2O. Also, the interaction energy of Zn^{2+}–$CF_3SO_3^-$ is lower than that of Zn^{2+}–H_2O, which verifies that zinc coordination has been reconstructed. The XRD result in Figure 10D shows that a similar $(002)_{Zn}$-dominated plane is observed in $Zn(CH_3SO_3)$ (Zn (MS)$_2$). $Zn(MS)_2$ can be taken as the replacement of the CF_3 in $Zn(CF_3SO_3)_2$ with the head group CH_3. However, if the length of two head groups is too long, such as $Zn(ES)_2$ and $Zn(DBS)_2$, (101) growth is induced. Hence, since the zinc deposition and texture behavior can be tuned by the electrolyte, it is important to choose suitable salt in AZB.

3.2 | Additives

Introducing an additive into an electrolyte is an effective strategy to regulate electrodeposition and mitigate side
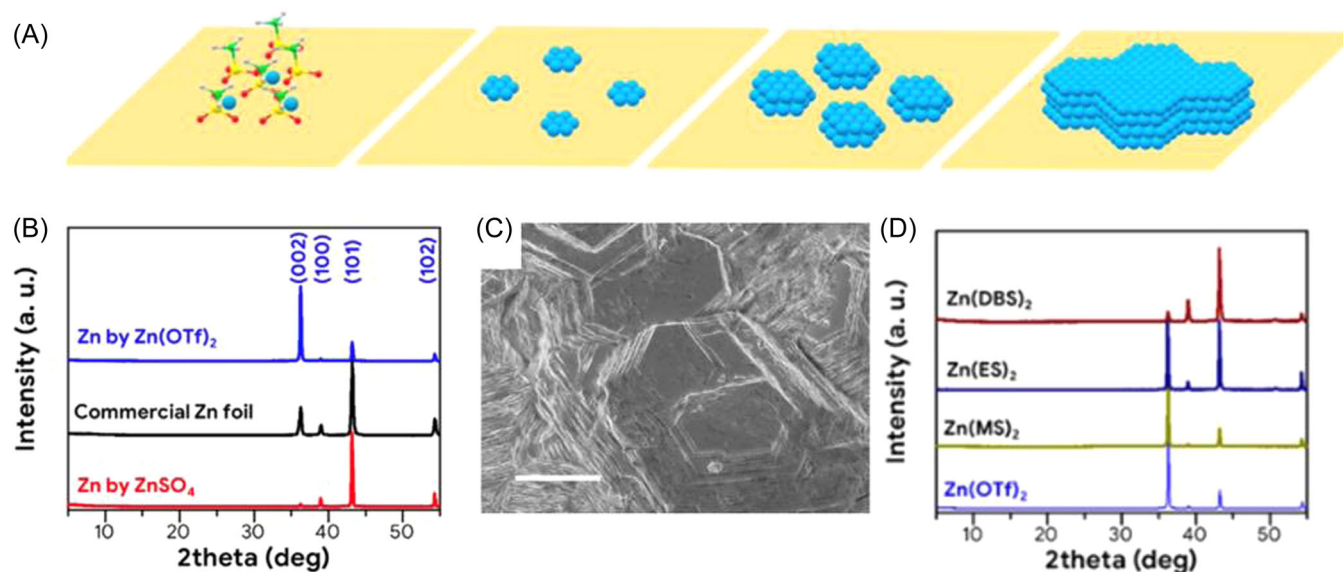
FIGURE 10 (A) Schematic of the SO_3^--based electrolyte inducing $(002)_{Zn}$ growth. (B) X-ray diffraction (XRD) patterns of electrodeposited Zn in $Zn(CF_3SO_3)_2$ and $ZnSO_4$. (C) Scanning electron microscope image of electrodeposited Zn in $Zn(CF_3SO_3)_2$. (D) XRD patterns of electrodeposited Zn in zinc dodecyl benzene sulfonate $Zn(DBS)_2$, zinc ethanesulfonate $Zn(ES)_2$, and $Zn(MS)_2$. Reproduced with permission, copyright Wiley.[135]

reactions. In addition, the additives are able to prevent the dissolution of the cathode material. Since this review only focuses on the interface between the anode and electrolyte, this latter part is not covered. As discussed, manipulating the zinc anode includes suppressing zinc dendrite growth and preventing side reactions. Generally, changes in the zinc anode surface such as dendrite formation are accompanied by side reactions; therefore, achieving a uniform and flat zinc anode surface can cut off the possibility of side reactions. The zinc electrolyte additive family can be divided into two parts: inorganic and organic additives. A summary of inorganic and organic additives is illustrated in Table 2.

3.2.1 | Inorganic additives

Inorganic additives including $NaSO_4$, $LiCl$, $LiClO_4$, boric acid, $InSO_4$, SnO_2, $Ce_2(SO_4)_3$, $La_2(SO_4)_3$, PbO, K_2SnO_3, lithium magnesium silicate (LMS) $((MgLi)_3Si_4O_{10}(OH)_{24} H_2O)$, $NiSO_4$, $CuSO_4$, and $PbSO_4$ can regulate zinc deposition in different ways.[136–144]

Building an electrostatic shield: Due to the electric field "tip effect," Zn ions tend to nucleate and deposit on protrusions. When specific cations with a reduction potential lower than Zn^{2+} are added, these cations preferentially aggregate on Zn protrusions instead, forming an electrostatic shield. The electrostatic shield has a positive electric field, which should prevent Zn^{2+} ions from further depositing on Zn protrusions. Thus, more uniform Zn electrodeposition can be achieved.[145,146] Wan et al.[147] added $NaSO_4$ in $ZnSO_4$ and found that it can suppress zinc dendrites, as evident in SEM images (Figure 11A,B). They hold the view that Na^+ has a lower reduction potential than Zn^{2+}, so during the Zn plating process, Na^+ will accumulate on the tip of zinc protuberances and form an electrostatic shield (Figure 11C). This positive electrostatic shield can repel Zn ions, hindering the further growth of the zinc dendrite. $LiClO_4$ has been

reported to have a similar function to inhibit zinc dendrite due to an electrostatic shield effect when it was added in $Zn(CF_3SO_3)_2$.[140] Generally, most of the work attributes the good performance of additives to cations. Guo et al.[148] have investigated the contribution of anions as well, that is, the addition of $LiCl$ to $ZnSO_4$. Although Li^+ can provide an electrostatic shield, other Li^+ salts such as Li_2SO_4 and $LiNO_3$ did not show the same flat morphology as $LiCl$, which is evident in the SEM images of Figure 11D–F. It was suggested that the addition of $LiCl$ may facilitate the formation of a nonconductive Li_2O/Li_2CO_3 layer, which blocks zinc dendrite formation, while other lithium salts produced a less-beneficial byproduct. Furthermore, Cl^- can encourage faster transport through the Li_2O/Li_2CO_3 layer.

Control the crystal orientation: A schematic of a hexagonal Zn crystal is shown in Figure 11G, illustrating the (002) planar facet. The orientation of Zn flakes influences the morphology of the Zn anode and the detailed orientation corresponding to the morphology type is illustrated in Figure 11H. In general, the smaller the angle between the zinc crystal and substrate, the less chance of Zn dendrite growth. The ideal angle is 0°–30° alignment to the substrate, corresponding to (002), (103), and (105) basal planes. This preferred orientation is beneficial for improving corrosion resistance and suppressing zinc dendrites. Intermediate planes like (114), (112), (102), and (101) mean that the angle of the zinc crystal and substrate is between 30° and 70°, while crystallographic planes (100) and (110) indicate that the angle is 70°–90°. These orientations are not favorable to inhibiting zinc corrosion due to their higher reactivity. Figure 11I reveals that the addition of indium sulfate, tin oxide, and boric acid could induce the preferential orientation of (002) and (103) planes, which are all basal planes.[141] The electrochemical performance of these additives also proved that the uniform electrodeposited zinc surface offers advantages for longer cycling life.

TABLE 2 Summary of different additives

| Additives	Advantages	Disadvantages
Inorganic additives	Build electrostatic shield Control crystal orientation Manipulate nucleation process Regulate solvation structure Increase polarization	High desolvation energy Sluggish Zn^{2+} mobility Low ionic conductivity
Organic additives	Regulate solvation structure Build electrostatic shield Inhibit Zn^{2+} 2D diffusion Control crystal orientation	Requirements for additive concentration optimization

Abbreviation: 2D, two dimensional.
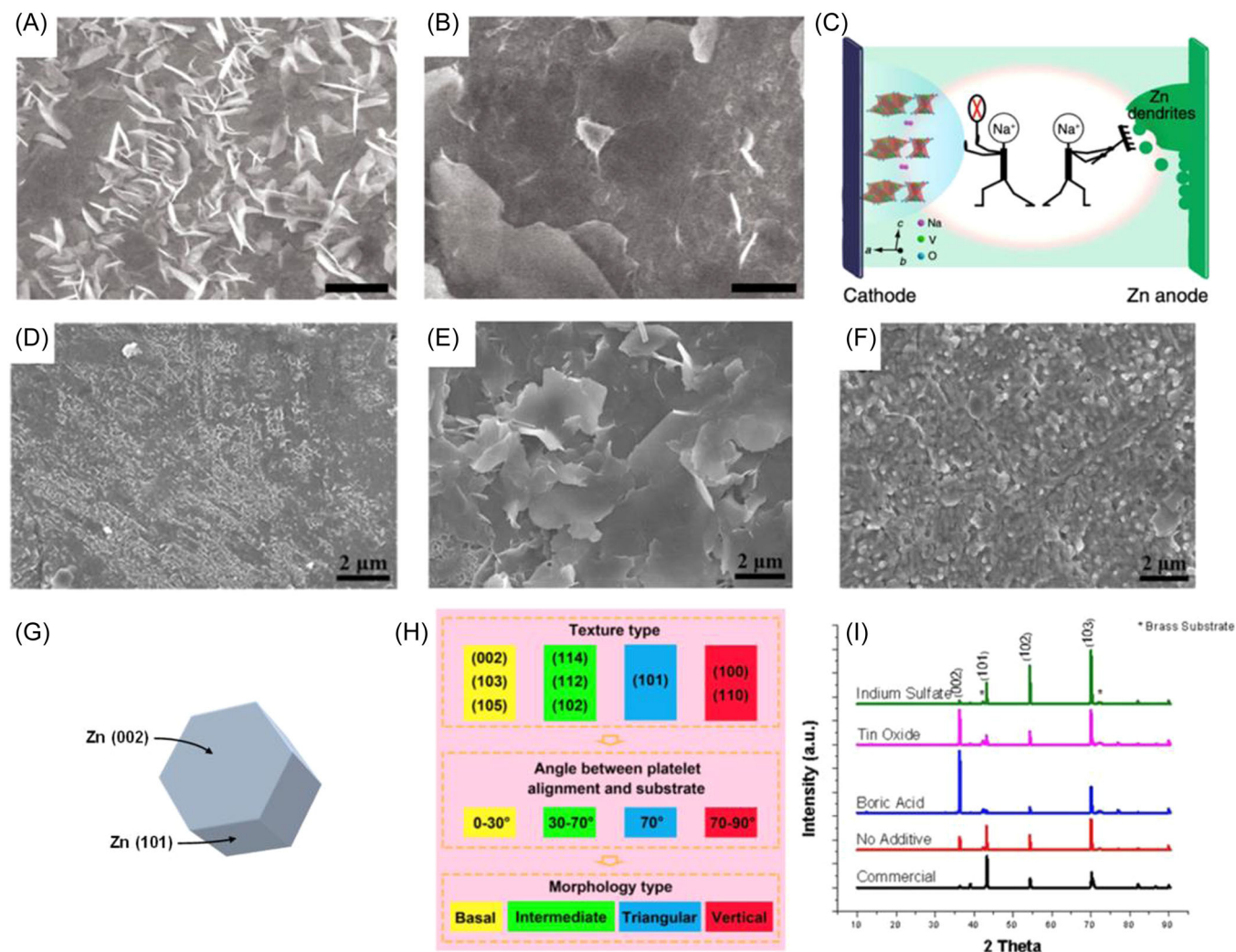
FIGURE 11 Scanning electron microscope (SEM) images of cycled Zn foil (A) without the additive and (B) with the NaSO$_4$ additive. (C) Schematic of the electrostatic shield. (A)–(C) Reproduced with permission, copyright Nature Portfolio.[147] SEM images of the Zn foil with (D) LiCl, (E) Li$_2$SO$_4$, and (F) LiNO$_3$ additives. Reproduced with permission, copyright American Chemical Society.[148] (G) Crystal faces of a Zn crystal. (H) Texture type of the Zn crystal with its corresponding morphology type. Reproduced with permission, copyright Elsevier.[46] (I) XRD patterns of the commercial Zn foil and Zn deposits with indium sulfate, tin oxide, and boric acid additives. Reproduced with permission, copyright Wiley.[141]

Manipulate the nucleation process: In general, the addition of the additive would act to increase the overpotential slightly. Although the rise of overpotential is generally not helpful for reversible zinc stripping/plating, an appropriate potential increase could affect the nucleation rate and related mechanism in a positive way. According to the classical nucleation model, the nucleation overpotential determines the number of active nucleation sites. More nucleation sites may lead to more uniform deposition, while fewer nucleation sites mean zinc deposited in limited places, which can favor the formation of zinc dendrites. Ce^{3+} has been introduced to the zinc electrolyte to form a hybrid Zn–Ce electrolyte.[138] In a potential versus time curve (Figure 12A), the Zn–Ce electrolyte shows higher overpotential than the pristine electrolyte, indicating more nucleation sites formed. Figure 12B,C shows SEM images of the zinc anode in the pristine electrolyte and Zn–Ce electrolyte. Notably, zinc will aggregate on limited sites and form undesirable dendrites over time in the pristine electrolyte. But in the Zn–Ce electrolyte, a large overpotential motivates more nucleation sites and thus promotes uniform deposition. Li et al.[138] also studied the nucleation mechanism by plotting $(I/I_{max})^2$ versus (t/t_{max}) in both electrolytes (Figure 12D). Based on the SH model, the nucleation from the Zn–Ce electrolyte conforms to a progressive mode, which means slow nucleation at many active sites, while zinc nucleation in the normal electrolyte matches with the instantaneous mode, which is fast nucleation at limited active sites. It is
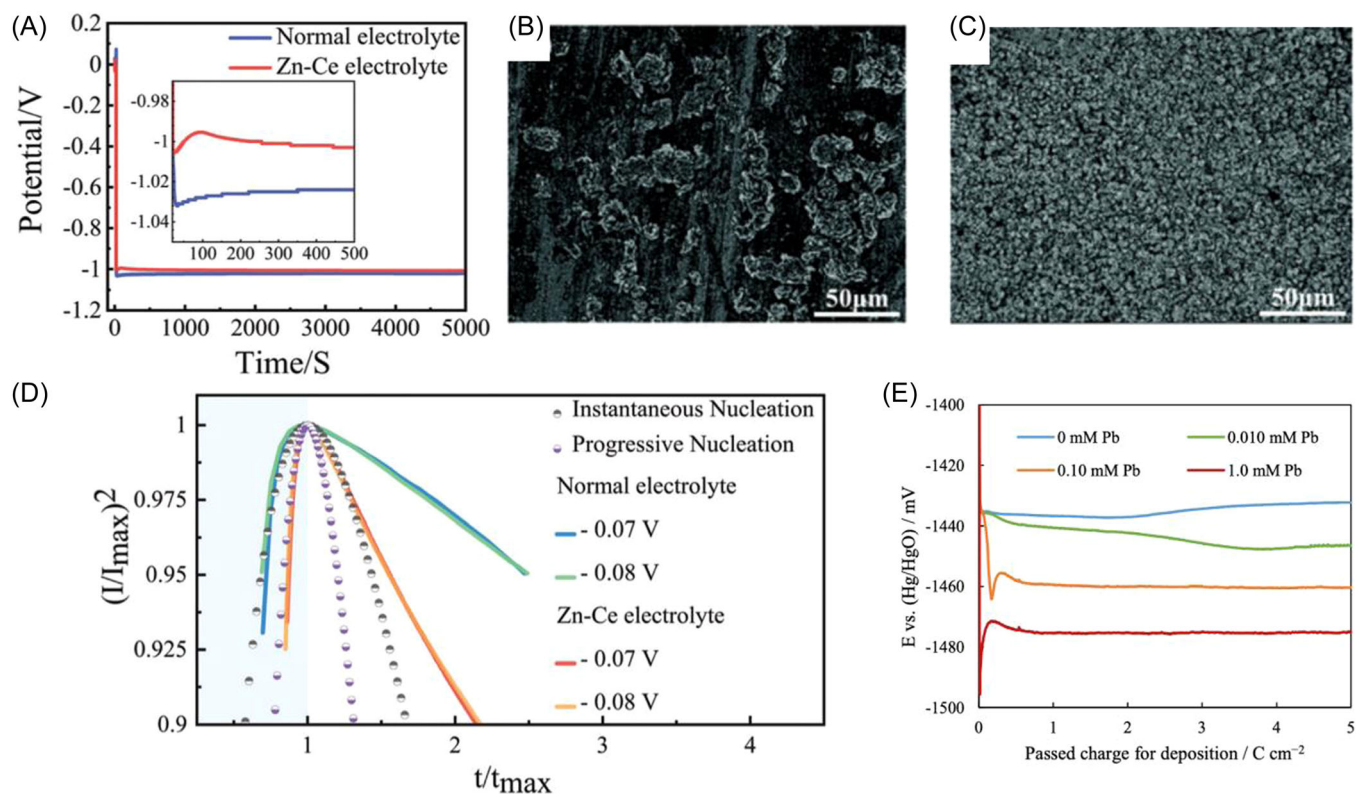
FIGURE 12 (A) Potential–time curve under galvanostatic deposition in normal and Zn–Ce electrolytes. Scanning electron microscope images of Zn electrodeposition in (B) normal electrolyte and (C) Zn–Ce electrolyte. (D) Theoretical $(I/I_m)^2 - (t/t_m)$ curves for instantaneous and progressive nucleation along with experimental data. (A)–(D) Reproduced with permission, copyright The Royal Society of Chemistry Publishing.[138] (E) Chronopotentiogram under galvanostatic deposition in the electrolyte with different amounts of the Pb additive. Reproduced with permission, copyright Elsevier.[149]

demonstrated that the addition of Ce^{3+} can change the nucleation mechanism from instantaneous to progressive nucleation. Yuan et al.[135] also reported that the addition of Pb ions to the zinc electrolyte shifts the initial nucleation potential to more negative (Figure 12E), thereby changing its nucleation behavior.

Regulate the solvation structure: It has been verified that the addition of LMS to $ZnSO_4$ can limit the solvation process of zinc due to its unique three-dimensional structure.[137] On a bare anode (Figure 13A), Zn dendrite growth and other parasitic reactions will occur. However, as shown in Figure 13B, the distinct structure of LMS can prevent the zinc solvation process, accelerating the activity of zinc ions and enhancing the electrochemical kinetics. As shown by Fourier transform infrared (FTIR) spectroscopy results in Figure 13C, the intensity of H_2O in-plane bending and stretching vibration reduces with the increasing amount of the LMS additive, which confirms the conversion of free water into absorbed water in LMS. This also means the suppressed formation of the zinc solvation structure $Zn(H_2O)_6^{2+}$ owing to the decreased free water. In addition, the activation energy of Zn^{2+} in $LMS + ZnSO_4$ is lower than in $ZnSO_4$, suggesting

that the desolvation process is easier in $LMS + ZnSO_4$ than in pure $ZnSO_4$. As a result, the Zn//Zn symmetrical battery in $LMS + ZnSO_4$ can retain 1000 h cycling duration at a current density of $0.5 \, mA \, cm^{-2}$ and capacity of $0.25 \, mAh \, cm^{-2}$.

Increase the polarization: The ionic conductivity of the electrolyte decreases after adding metallic salt due to the different mobilities of metal ions, which may increase polarization and slow down the deposition of zinc. Zinc dendrites are not likely to form at a slow deposition rate. Chang et al.[139] have tested the voltammetry behavior of the electrolyte with additives of $NiSO_4$, $CuSO_4$, and $PbSO_4$, as shown in Figure 13D. It is found that the onset deposition potential (E_{IP}) of the electrolyte increases when Pb^{2+} and Ni^{2+} are added, while reduction potential (E_{IP}) decreases after introducing Cu^{2+}. Since E_{IP} can be used as the indicator for judging the polarization extent of the electrolyte, they found that the addition of Pb^{2+} and Ni^{2+} leads to high polarization, whereas Cu^{2+} plays a depolarization role. As a result, the high polarization that Pb^{2+} and Ni^{2+} provide can suppress zinc dendrite growth by reducing the deposition rate. Conversely, depolarization that is associated with Cu^{2+} promotes serious HER.
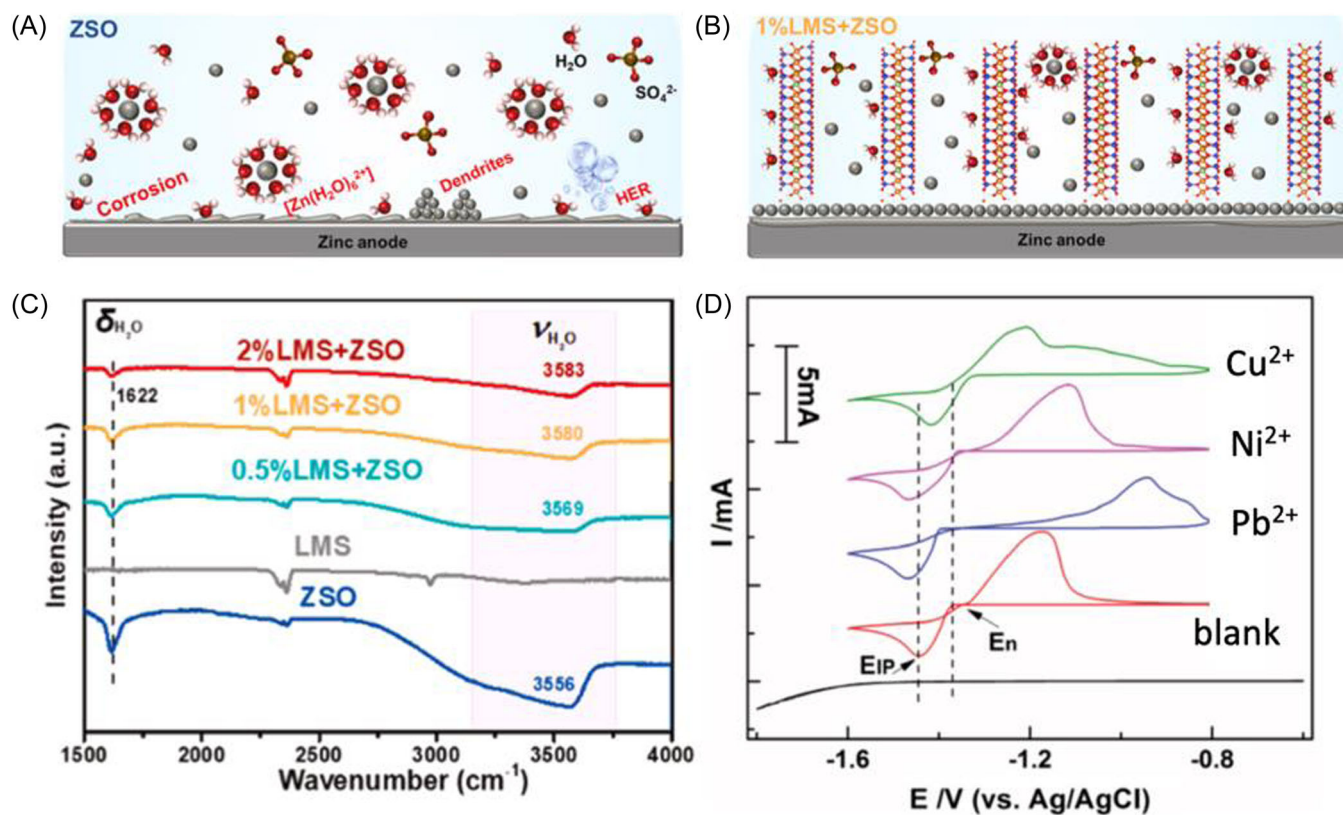
FIGURE 13 Schematic of Zn^{2+} in (A) $ZnSO_4$ (ZSO) and (B) LMS + $ZnSO_4$ electrolytes. (C) Fourier transform infrared of $ZnSO_4$ and LMS + $ZnSO_4$ electrolytes. Reproduced with permission, copyright Elsevier.[137] (D) Voltammetry behavior of the blank electrolyte and with additives. Reproduced with permission, copyright Wiley.[139]

3.2.2 | Organic additives

Based on the state of organic additives, they could be divided into two types: a solid organic additive soluble in water and a liquid organic additive miscible with water. The solid organic additive includes cationic surfactants (such as dodecyltrimethylammonium chloride and benzyl-trimethylammonium chloride), anionic surfactants (such as sodium dodecyl sulfate [SDS] and sodium dodecyl benzene sulfonate), and polymer (such as polyethyleneimine and polyethylene glycol [PEG]).[49,111,127,150–168] Liquid organic additives are polar solvents including dimethyl carbonate (DMC), ethylene glycol (EG), diethyl ether (Et$_2$O), dimethyl sulfoxide (DMSO), acetonitrile (AN), and so on.[9,50,51,169–179] Since both solid and liquid organic additives are soluble in water, the functions of these two additives are similar, so these two additives will not be discussed separately in this chapter. Generally, organic additives can regulate the Zn anode in the following way.

Regulate the solvation structure: Generally, the solvation sheath of the Zn^{2+} ion in the aqueous weak acidic electrolyte is $Zn(H_2O)_6^{2+}$, which is the root of dendrite formation and parasitic reaction, as the solvated structure $Zn(H_2O)_6^{2+}$ has a high energy barrier for the zinc ion to overcome and nucleate on the anode surface. Thus, if other molecules can replace H_2O in $Zn(H_2O)_6^{2+}$, the Zn^{2+}–H_2O bond energy will decrease, leading to a weaker solvation effect. Hou et al.[171] introduced an AN additive into the $ZnSO_4$ electrolyte and found that the Zn symmetrical battery could cycle for 650 h at 2 mA cm^{-2} with a capacity of 2 mAh cm^{-2}. They attributed the excellent cycling performance to the modification of the Zn^{2+} solvation structure. By conducting molecular dynamics simulation, it was demonstrated that the incorporation of AN in the zinc electrolyte could change the zinc solvation structure into three new types of solvation structure: $Zn(H_2O)_5(AN)_1^{2+}$, $Zn(H_2O)_4(AN)_2^{2+}$, and $Zn(H_2O)_3(AN)_3^{2+}$.[171] Thus, AN can substitute a maximum of three water molecules in the original sheath and achieve $Zn(H_2O)_3(AN)_3^{2+}$, the structure of which is shown in Figure 14A. This new solvation structure results in moderate desolvation energy and enhanced Zn^{2+} mobility. Other organic additives such as glucose, DMK, and DMC have also been substantiated by experimental and computational evidence that they too can replace water molecules in the $Zn(H_2O)_6^{2+}$ structure and thus weaken solvation energy.[50,177]

Chang et al.[178] have introduced EG into the $ZnSO_4$ electrolyte and have calculated the binding energy
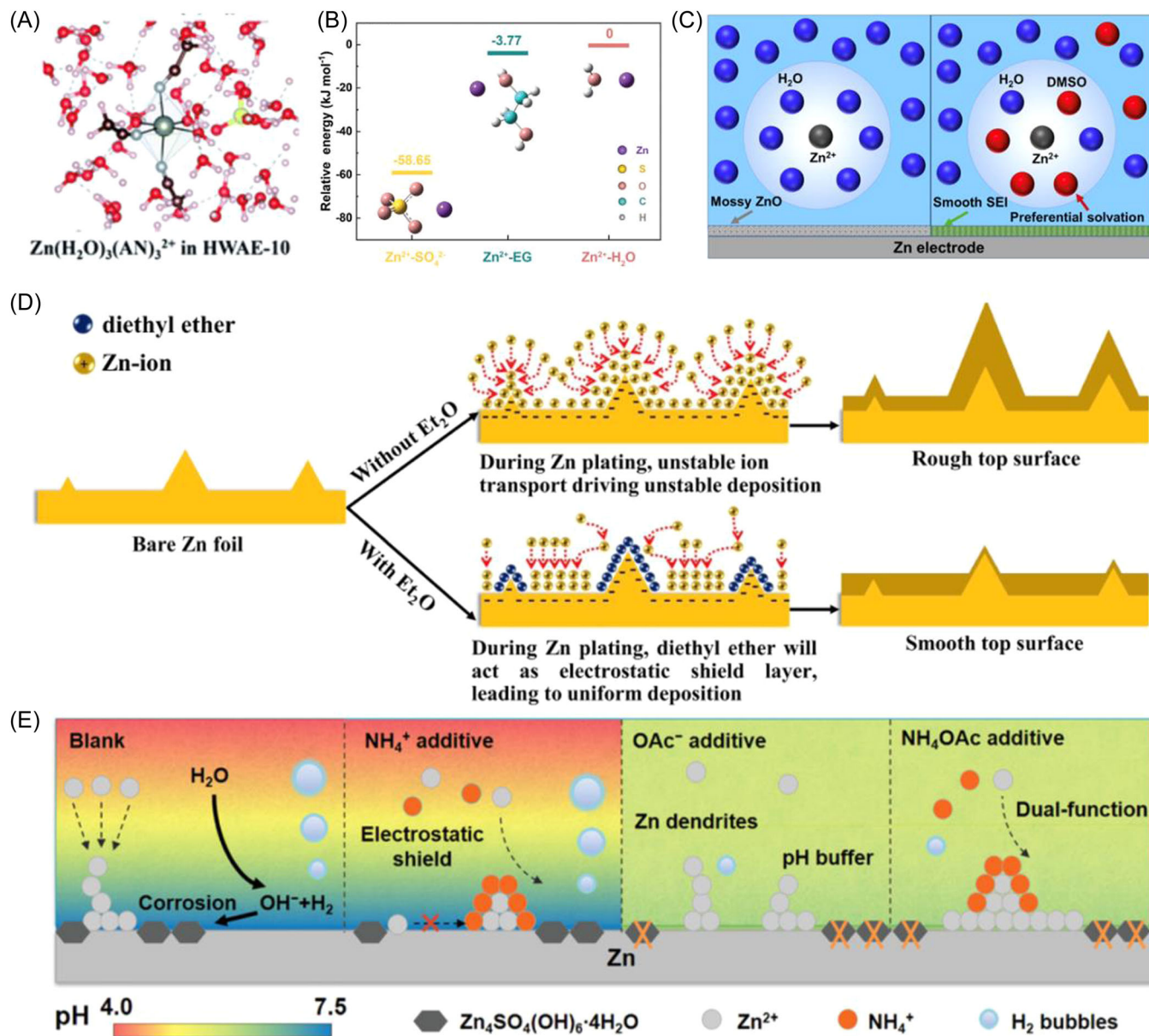
FIGURE 14 (A) Illustration of the $Zn(H_2O)_3(AN)_3^{2+}$ structure. Reproduced with permission, copyright RSC Publishing.[171] (B) Relative binding energy for Zn^{2+} with different species obtained from DFT calculations. Reproduced with permission, copyright The Royal Society of Chemistry Publishing.[178] (C) Schematic of the Zn^{2+} solvation structure and zinc surface passivation in H_2O and H_2O-dimethyl sulfoxide solvents. Reproduced with permission, copyright American Chemical Society.[51] (D) Illustration of diethyl ether additives as an electrostatic shield. Reproduced with permission, copyright Elsevier.[179] (E) Schematic of the self-regulation NH_4OAc additive. Reproduced with permission, copyright Wiley.[180]

between Zn^{2+} ions and other anion/solvents (SO_4^{2-}, EG, H_2O) to further understand the solvation structural changes. The result displayed in Figure 14B shows that binding energy is ranked as follows: $Zn^{2+}-SO_4^{2-} > Zn^{2+}-EG > Zn^{2+}-H_2O$, implying that Zn^{2+} ions are inclined to coordinate with EG rather than H_2O. After EG is inserted into $Zn^{2+}-5H_2O$, its electrostatic potential has reduced by 25.1 kcal mol^{-1}, suggesting the reduction of electrostatic repulsion and fast transport of Zn^{2+}. Also, EG could enhance the H bonding between EG and H_2O,

providing a pathway for operating zinc ion batteries at a low temperature.

Cao et al.[51] have reported that the interaction of DMSO and the electrolyte could not only modify the solvation structure like other organic additives but it can also form a dense SEI-like layer on the anode. The working mechanism of DMSO is shown in Figure 14C. DMSO is reduced during zinc plating and a $Zn_{12}(SO_4)_3Cl_3(OH)_{15} \cdot 5H_2O-ZnSO_3-ZnS$ layer is generated on the anode, which can prevent the decomposition of solvated

water. Due to the dual effect of the optimized solvation structure and formed SEI layer, the CE of Zn depositing/dissolving can maintain ~100% after 400 h cycling.

Build an electrostatic shield: Like inorganic additives, which are usually metal ions, some organic cations can also adsorb on the tip and establish an electrostatic shield to overcome the tip effect. For example, tetrabutylammonium (TBA^+) has been suggested to raise the energy barrier of the Zn^{2+} ion due to the shielding effect.[49,162] Other organic molecules share a similar effect to metal ions as they are polar and thus can be preferably attracted to Zn tips under high local current density. Highly polarized Et_2O is a typical example.[179] As reported, the initial Zn morphology was coarse, but after adding 2 vol% in the electrolyte, the Zn dendrites were reduced and the Zn surface was flattened. The schematic of the whole process is illustrated in Figure 14D.

Han et al.[180] have reported a dual-functional additive NH_4OAc that not only could establish an electrostatic shield but also has the ability to maintain an interface pH value. As is shown in Figure 14E, NH_4^+ plays an important role in establishing the electrostatic shield, while OAc^- adjusts the electrolyte pH and keeps it at ~5.14. This pH buffer mitigates side reactions and reduces insoluble side product formation. Therefore, through the dual function of NH_4^+ and OAc^-, this modified electrolyte can achieve both a flat zinc surface and a reduction of chemical side reactions.

Inhibit the 2D diffusion of Zn^{2+} ions: PEG has been reported to have the ability to inhibit rapid 2D diffusion of Zn^{2+} ions. A comparison of the control electrolyte and electrolyte with the PEG additive is displayed in Figure 15A.[168] In the control electrolyte, Zn^{2+} ions tend to laterally self-diffuse on the anode to find the minimum free energy sites to nucleate and transfer electrons. Generally, these energetically favorable sites are dislocations, impurities, and grain boundaries. At subsequent deposition periods, Zn^{2+} ions will deposit at existing nucleation sites, which leads to large dendrite growth. However, for electrolytes with the PEG additive, PEG is absorbed on the anode surface, which can be taken as a physical barrier for the 2D diffusion of Zn^{2+} ions. Thus, more nucleation sites were achieved and a large number of small dendrites could be observed in the PEG electrolyte, while a small number of large dendrites were formed in the control electrolyte. In addition to PEG, other organic additives like vanillin and Sac have been reported to have a similar effect.[165,182]

Control crystal orientation: Organic additives can also control zinc crystal orientation by altering surface energy. Sun et al.[161] have found that different additives can produce different surface structures, with the associated XRD diffractogram shown in Figure 15B. It suggests that the addition of cetyltrimethylammonium bromide (CTAB), SDS, and thiourea (TU) favors the orientation of (101) zinc, while with the PEG additive, deposited Zn produces strong peaks at (002) and (103). As mentioned before, (101) supports zinc crystal growth at 70° to the surface, thus zinc dendrites are still likely to grow with the additive of CTAB, SDS, and TU. Since (002) and (103) support a zinc basal plane, which is parallel to the electrode, zinc dendrites can be suppressed with the PEG additive. Other researchers have utilized DFT computational modeling to understand the mechanism. Feng et al.[174] calculated the absorption energy of a (002) plane to DMSO and H_2O. The results in Figure 15C show that the binding energy of (002) Zn to DMSO is higher than that of water and it demonstrates that DMSO is thus likely to induce (002) growth. Sorbitol (SBT) is another organic additive that could guide (002) plane growth[181] and the XRD pattern of Zn deposited in the SBT additive is shown in Figure 15D. The absorption energy of SBT with different Zn crystal planes was also studied. According to Figure 15E–G, the binding energy of SBT with (002) exhibits the lowest value (−0.557 eV) compared to (100) and (101) planes, indicating that SBT could encourage more (002) zinc planes to be exposed.

It is worth noting that the introduction of organic additives may cause other problems: (1) Some organic additives can replace water molecules in the original Zn^{2+} solvation sheath to form a new solvation structure. But if the new solvated Zn^{2+} sheath has a large radius, more energy needs to be consumed for Zn^{2+} to desolvate than in $Zn(H_2O)_6^{2+}$. (2) Although new hydrated Zn^{2+} complexes could form, there will still be remaining $Zn(H_2O)_6^{2+}$ and Zn^{2+}-anions in the electrolyte, which increases the desolvation energy and can lead to sluggish Zn^{2+} transport. (3) The addition of the additive will reduce the relative water content in the electrolyte and will thus decrease the ionic conductivity of the electrolyte, which has a detrimental effect on battery performance.

3.3 | Concentration

The concentration of the electrolyte has a great impact on the zinc plating/stripping ability.[107,183–185] As mentioned earlier, the regular aqueous zinc solvation sheath is $Zn(H_2O)_6^{2+}$. An increasing Zn^{2+} concentration should reduce the relative availability of water molecules to complete the solvation structure, thereby lowering the energy barrier and facilitating zinc desolvation. Generally, the concentrated electrolyte favors forming dense and uniform zinc layers. Zheng et al.[72] studied zinc deposition morphology in the dilute electrolyte (0.05 M $ZnSO_4$) and concentrated electrolyte (2.5 M $ZnSO_4$). The SEM images in Figure 16A,B
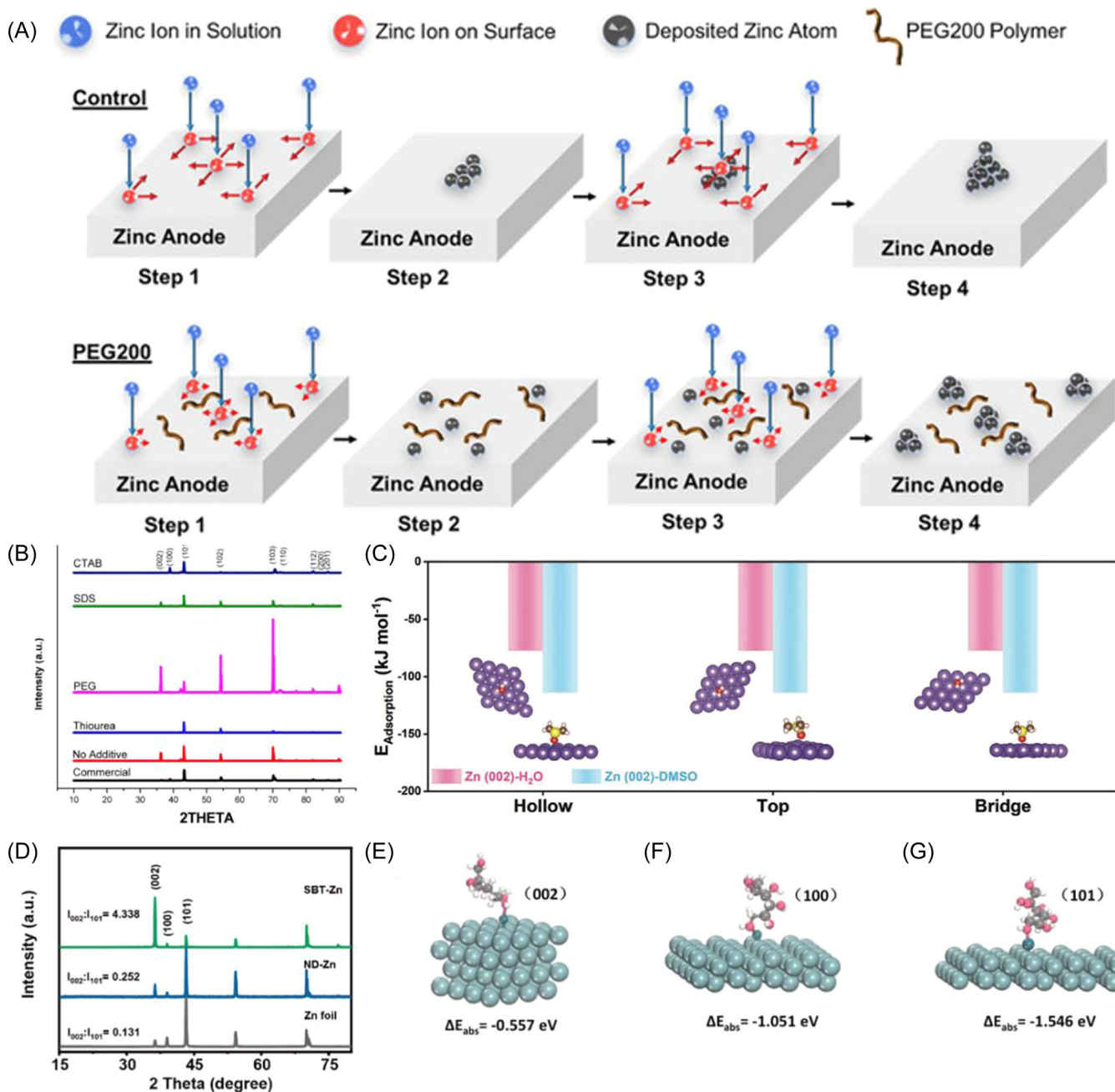
FIGURE 15 (A) Schematics of Zn deposition without (top) and with (bottom) a two-dimensional (2D) diffusion limit, following the inclusion of the polyethylene glycol additive. Reproduced with permission, copyright Wiley.[168] (B) X-ray diffraction (XRD) patterns of the zinc anode electrodeposited in the electrolyte with and without organic additives and commercialized zinc. Reproduced with permission, copyright American Chemical Society.[161] (C) Binding energy of the Zn (002) plane with H_2O or DMSO. Reproduced with permission, copyright Wiley.[174] (D) XRD patterns of the pure Zn foil and Zn electrodeposition in $ZnSO_4$ and $ZnSO_4$–SBT electrolytes with a current density of $20\,mA\,cm^{-2}$ for 0.5 h. Absorption energy comparison for Zn with the Zn^{2+}–SBT coordination compound at the crystallographic orientations of (E) (002), (F) (100), and (G) (101) planes. (D)–(G) Reproduced with permission, copyright Elsevier.[181]

show that, under the same deposition voltage, leaf-like and branched zinc dendrites were observed in the dilute electrolyte, while no obvious zinc dendrite can be found in the concentrated electrolyte. A kinetic rate-limited model can explain the mechanism. Figure 16C illustrates that for a dilute solution, there are not enough ions to replenish those depleted by the surface reaction. Therefore, the near-surface area forms a thick ion depletion region, and leaf-like dendrites are likely to grow in this region. But the concentrated electrolyte has a thin diffusion layer, which is easy for deposited Zn to overcome the mass-transfer limitation (Figure 16D).
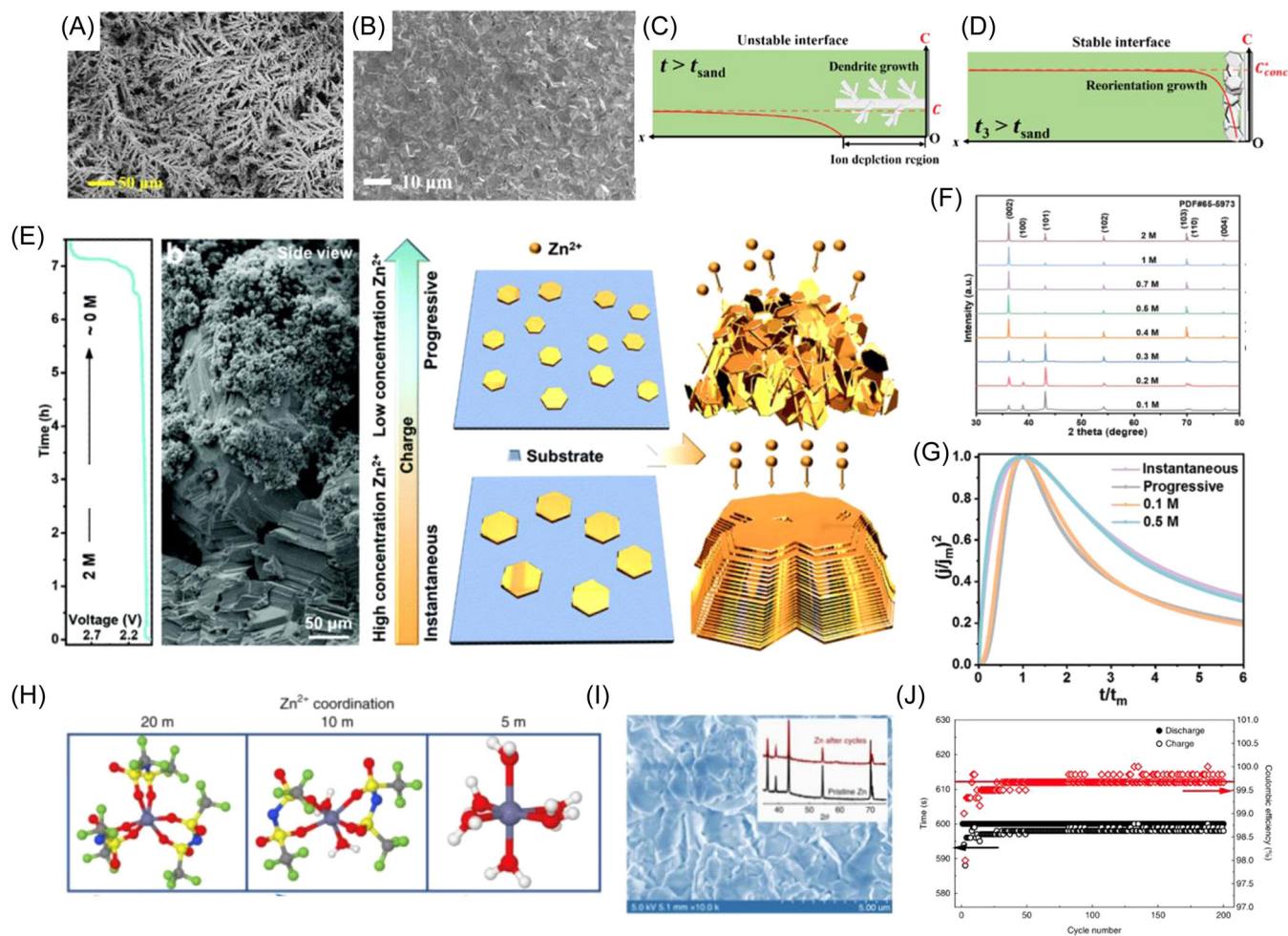
FIGURE 16 Scanning electron microscope (SEM) image of Zn electrodeposits in (A) 0.05 M and (B) 2.5 M ZnSO$_4$ electrolytes when deposited at −1.9 V. Schematic of Zn electrodeposits in (C) dilute and (D) concentrated electrolytes. (A)–(D) Reproduced with permission, copyright American Association for the Advancement of Science.[72] (E) SEM image and schematic of Zn deposition at decreasing concentration. (F) X-ray diffraction (XRD) results of Zn deposits in different concentration electrolytes. (G) Theoretical $(I/I_m)^2 - (t/t_m)$ plots for instantaneous and progressive nucleation and experimental data of different concentrated electrolytes. (E)–(G) Reproduced with permission, copyright The Royal Society of Chemistry Publishing.[186] (H) Representative Zn^{2+} coordination in 1 M Zn(TFSI)$_2$ with 20 M, 10 M, and 5 M LiTFSI additives. (I) SEM and XRD results of the Zn electrode after 500 cycles in 1 M Zn(TFSI)$_2$ + 20 M LiTFSI. (J) Cycling performance and CE of Zn/Pt at 1 mA cm^{-2}. (H)–(J) Reproduced with permission, copyright Springer Nature.[187]

In addition to zinc dendrites, Zn^{2+} concentration also has an influence on Zn crystal orientation. The orientation of deposited Zn in 0.1 to 2 M electrolytes has been investigated.[186] According to the SEM images (Figure 16E) and XRD patterns (Figure 16F), for the electrolyte with concentration ≤0.3 M, Zn deposits exhibit a mossy morphology and are (101)-dominated. If the electrolyte concentration is ≥0.4 M, electrodeposited Zn is blocky and exhibits a (200) dominated morphology. To explore it in depth, nucleation modes in relatively high concentration (0.5 M) and low concentration (0.1 M) electrolytes have been studied. Figure 16G exhibits the curve between $(I/I_{max})^2$ and (t/t_{min}) for these two electrolytes. This

indicates that the nucleation mode is progressive for relatively low-concentration electrolytes (≤0.3 M) and instantaneous for higher-concentration electrolytes (≥0.4 M). Therefore, different concentrations lead to altered nucleation patterns.

Recently, a novel electrolyte called "water in salt," that is, an extremely concentrated electrolyte, has been proposed.[187–191] In this electrolyte, there is less solvated water around Zn^{2+} and less free water in the electrolyte, which could lead to flat Zn deposition and fewer side reactions. Wang et al.[187] developed a "water in salt" electrolyte (1 M Zn(TFSI)$_2$ + 20 M LiTFSI). Notably, as the concentration of TFSI$^-$ grows, the water molecules in solvated Zn^{2+} gradually decrease and the quantity of

TFSI$^-$ increases, as shown in Figure 15H. When TFSI$^-$ concentration reaches 20 M, solvated waters coordinated to Zn^{2+} have been completely replaced by TFSI$^-$. Due to the presence of less water, parasitic corrosion reactions were inhibited, which is evidenced by no byproduct formation (Figure 16I). The CE of the zinc anode can maintain ~100% by preventing Zn corrosion and inhibiting HER, as shown in Figure 16J. However, such electrolytes are difficult to mass produce due to their high price. ZnCl$_2$ is another promising candidate for the "water in salt" electrolyte due to its low price and high solubility. Compared with 3 M ZnSO$_4$, 20 M ZnCl$_2$ can suppress side reactions and form a dense interface layer on the zinc anode, which blocks zinc dendrite growth.[191]

4 | SUMMARY AND PERSPECTIVE

Rechargeable AZBs, which are undergoing rapid development, have gained extensive attention in recent years due to their remarkable advantages including high specific theoretical capacity, excellent volumetric capacity, low fabrication cost, and compatibility with aqueous electrolytes. However, AZBs still have a series of challenges, such as cathode material dissolution, electrolyte consumption, and Zn anode instability. In this review, we have concentrated on the issues related to the Zn anode, which involves physical and chemical instability. For physical instability, the dendrite starts from the initial nucleation mechanism to further growth and secondary nucleation. In addition to nucleation, crystal orientation and other external factors like current density and temperature have an influence on dendrite morphology. For chemical instability, several fundamental parasitic reactions occur when Zn is in contact with the aqueous electrolyte, including Zn corrosion, hydrogen evolution, and resulting byproduct generation. Regarding the issues discussed above, the factors affecting Zn electrodeposition are considered to be the electrical field, Zn^{2+} ion solvation structure, or sluggish Zn ion transport. These factors are highly related to the electrolyte. Thus, by manipulating the electrolyte, the favorable regulation of the Zn anode can be achieved.

We summarize three strategies for how electrolytes can tune the Zn electrodeposition: the optimization of salts, additives, and electrolyte concentration, as shown in Figure 17. After examining most Zn electrolyte salts, it is known that the selection of salt has a great influence on Zn crystal orientation and dendrite suppression. When it comes to additives, there are two types: inorganic additives and organic additives. Inorganic additives generally tune Zn electrodeposition by building an electrostatic shield, increasing polarization, manipulating nucleation, controlling crystal orientation, and regulating solvation structure. Organic additives have the ability to build an electrostatic shield, control crystal orientation, inhibit Zn^{2+} 2D diffusion, and regulate solvation structure. The last electrolyte strategy is concentration optimization. Generally, increasing concentration could lead to a better-oriented and denser Zn layer; however, it could also lead to poor ionic conductivity and high viscosity, which is not ideal for Zn electrodeposition. Therefore, a balance should be found to achieve high-performance AZBs.

Although a great deal of work has been done to understand Zn anode issues and related electrolyte manipulation methods, there are still some areas that need to be resolved:

(1) The theory of nucleation during galvanostatic deposition. In the classical nucleation theory, nearly all research is based on the potentiostatic deposition, with the SH model being the most typical. It divides the nucleation process into two types: instantaneous and progressive nucleation. However, most battery tests are performed under galvanostatic conditions. Previous studies are not sufficient to support galvanostatic research. Although there have been some attempts, these models have not been widely applied and verified.

(2) Quantitative measurement of Zn dendrites and parasitic reactions. Researchers normally attribute AZB capacity decay to the formation of Zn dendrites and parasitic reactions. But most postmortem studies lack quantitative analysis, and thus, it is still inclusive of how much of Zn dendrites are formed, how much of Zn is corroded, and how much gas is created during the charging/discharging period. In future work, TEM imaging or X-ray computed tomography could be used to delineate the relative importance of these failure modes. In addition, titration gas chromatography and DEMS are helpful to determine the volume of generated H$_2$.

(3) In situ characterization of Zn electrodeposition and the anode–electrolyte interface. Ex situ experiments may be influenced by sample contamination and product reaction with the atmosphere. In situ characterization provides an accurate understanding of Zn electrodeposition processes and any influence from changing the electrolyte. In situ optical microscopy, XRD, SEM, TEM, and atomic force microscopy can all be used to monitor dynamic changes in the formation, morphology, crystallinity, and chemical composition of Zn electrodeposition,
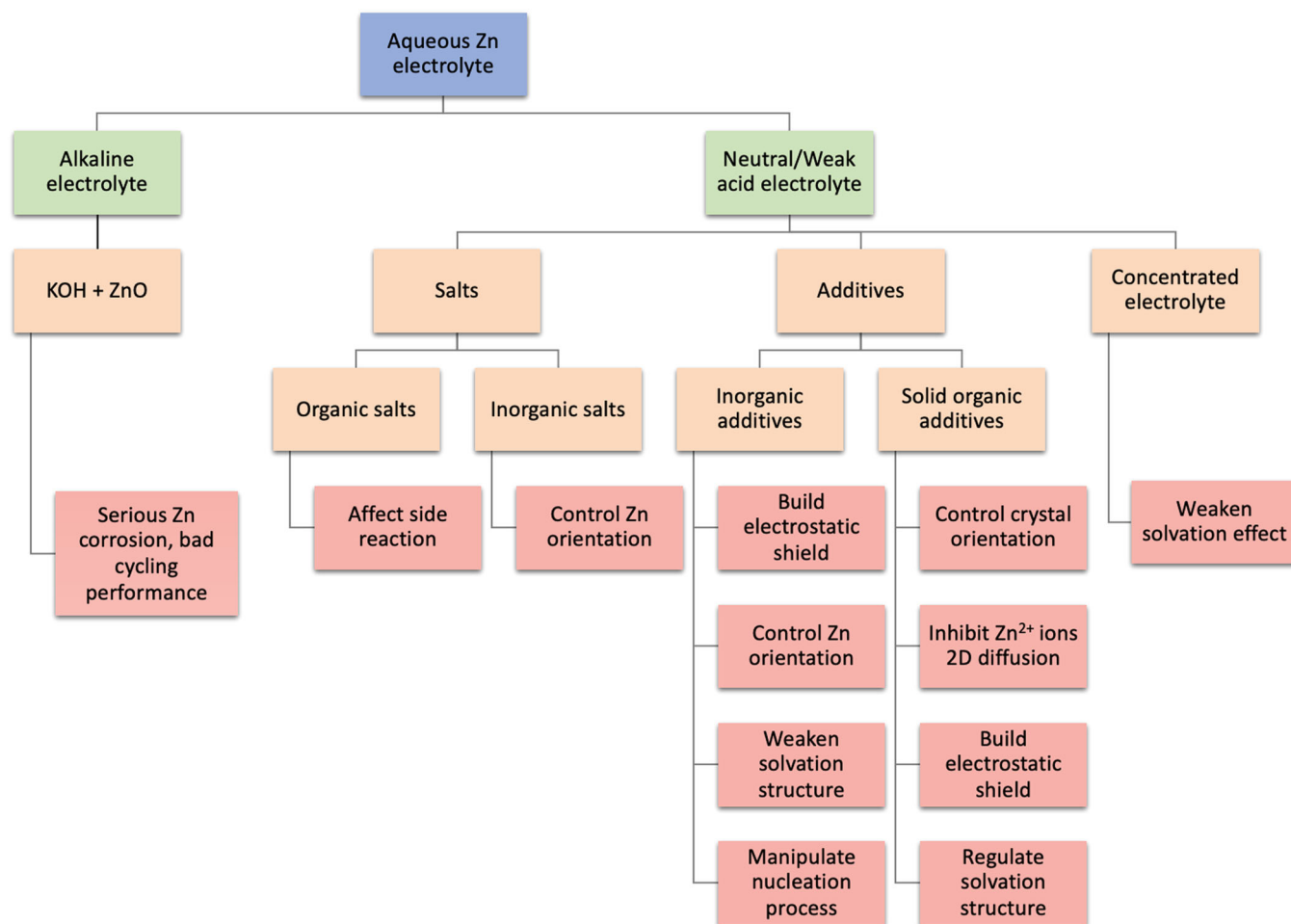
FIGURE 17 Summary of the mechanism of electrolyte engineering to regulate the Zn anode

providing a better understanding of its mechanism. In situ Raman, FTIR, and X-ray absorption spectroscopy could be used to track the evolution, solvation structure, ionic transport, and chemical reaction at the anode–electrolyte interface, which could open avenues for fabricating effective electrolytes.

(4) Integrated design for electrolytes. In general, optimizing electrolytes to solve one specific issue can cause unintended secondary problems. For example, the introduction of the additive could suppress Zn dendrite formation but also inhibit Zn^{2+} transportation due to the increased energy barrier. Also, more concentrated electrolytes can induce denser Zn electrodeposition but also decreases the ionic conductivity. Thus, mitigating a single issue is not enough. The integrated design of the electrolyte is necessary to balance all the issues that need to be solved.

Taken together, this review provides a new perspective on electrolyte strategies to regulate the zinc metal anode. Further research is needed to understand the electrodeposition mechanism of zinc and the regulation mechanism of the electrolyte.

CONFLICT OF INTEREST
The authors declare no conflict of interest.

ORCID
Alex W. Robertson [ORCID] http://orcid.org/0000-0002-9521-6482

REFERENCES
1. Liu K, Liu Y, Pei A, Cui Y. Materials for lithium-ion battery safety. *Sci Adv.* 2018;4(6):sciadv.aas9820.
2. Gong C, Pu SD, Gao X, et al. Revealing the role of fluoride-rich battery electrode interphases by operando transmission electron microscopy. *Adv Energy Mater.* 2021;11(10):2003118.

3. Biswal P, Stalin S, Kludze A, Choudhury S, Archer LA. Nucleation and early stage growth of Li electrodeposits. *Nano Lett.* 2019;19(11):8191-8200.

4. Gao X, Zhou Y-N, Han D, et al. Thermodynamic understanding of Li-dendrite formation. *Joule.* 2020;4(9):1864-1879.

5. Ghazi ZA, Sun Z, Sun C, et al. Key aspects of lithium metal anodes for lithium metal batteries. *Small.* 2019;15(32):1900687.

6. Zuo Y, Wang K, Pei P, et al. Zinc dendrite growth and inhibition strategies. *Mater Today Energy.* 2021;20:100692.

7. Ho VC, Lim H, Kim MJ, Mun J. Improving the performance of aqueous zinc-ion batteries by inhibiting zinc dendrite growth: recent progress. *Chem Asian J.* 2022;17:e202200289.

8. Hoang Huy VP, Hieu LT, Hur J. Zn metal anodes for Zn-ion batteries in mild aqueous electrolytes: challenges and strategies. *Nanomaterials.* 2021;11(10):2746.

9. Qin R, Wang Y, Zhang M, et al. Tuning Zn^{2+} coordination environment to suppress dendrite formation for high-performance Zn-ion batteries. *Nano Energy.* 2021;80:105478.

10. Wu X, Markir A, Xu Y, et al. A rechargeable battery with an iron metal anode. *Adv Funct Mater.* 2019;29(20):1900911.

11. Jiang J, Liu J. Iron anode-based aqueous electrochemical energy storage devices: recent advances and future perspectives. *Interdiscip Mater.* 2022;1:116-139.

12. Liang G, Mo F, Yang Q, et al. Commencing an acidic battery based on a copper anode with ultrafast proton-regulated kinetics and superior dendrite-free property. *Adv Mater.* 2019;31(52):1905873.

13. Gallagher TC, Sandstrom SK, Wu C-Y, et al. Copper metal electrode reversibly hosts fluoride in a 16 m KF aqueous electrolyte. *Chem Commun.* 2022;58:10218-10220.

14. Liu J, Dong D, Caro AL, et al. Aqueous electrolytes reinforced by Mg and Ca ions for highly reversible Fe metal batteries. *ACS Cent Sci.* 2022;8(6):729-740.

15. Ming J, Guo J, Xia C, Wang W, Alshareef HN. Zinc-ion batteries: materials, mechanisms, and applications. *Mater Sci Eng R.* 2019;135:58-84.

16. Wang L, Zheng J. Recent advances in cathode materials of rechargeable aqueous zinc-ion batteries. *Mater Today Adv.* 2020;7:100078.

17. Konarov A, Voronina N, Jo JH, Bakenov Z, Sun YK, Myung ST. Present and future perspective on electrode materials for rechargeable zinc-ion batteries. *ACS Energy Lett.* 2018;3(10):2620-2640.

18. Li Y, Fu J, Zhong C, et al. Recent advances in flexible zinc-based rechargeable batteries. *Adv Energy Mater.* 2018;9(1):1802605.

19. Yu P, Zeng Y, Zhang H, Yu M, Tong Y, Lu X. Flexible Zn-ion batteries: recent progresses and challenges. *Small.* 2019;15(7):1804760.

20. Song M, Tan H, Chao D, Fan HJ. Recent advances in Zn-ion batteries. *Adv Funct Mater.* 2018;28(41):1802564.

21. Fang G, Zhou J, Pan A, Liang S. Recent advances in aqueous zinc-ion batteries. *ACS Energy Lett.* 2018;3(10):2480-2501.

22. Xu W, Wang Y. Recent progress on zinc-ion rechargeable batteries. *Nano-Micro Lett.* 2019;11:90.

23. Yi Z, Chen G, Hou F, Wang L, Liang J. Strategies for the stabilization of Zn metal anodes for Zn-ion batteries. *Adv Energy Mater.* 2020;11(1):2003065.

24. Qian G, Zan G, Li J, et al. Structural, dynamic, and chemical complexities in zinc anode of an operating aqueous Zn-ion battery. *Adv Energy Mater.* 2022;12(21):2200255.

25. Ye X, Saqib M, Mao J, Li G, Hao R. Spatiotemporally super-resolved dendrites nucleation and early-stage growth dynamics in zinc-ion batteries. *Cell Rep Phys Sci.* 2021;2(5):100420.

26. Yang Q, Li Q, Liu Z, et al. Dendrites in Zn-based batteries. *Adv Mater.* 2020;32(48):2001854.

27. Wang K, Pei P, Ma Z, et al. Dendrite growth in the recharging process of zinc–air batteries. *J Mater Chem A.* 2015;3(45):22648-22655.

28. Yufit V, Tariq F, Eastwood DS, et al. Operando visualization and multi-scale tomography studies of dendrite formation and dissolution in zinc batteries. *Joule.* 2019;3(2):485-502.

29. Sasaki Y, Yoshida K, Kawasaki T, Kuwabara A, Ukyo Y, Ikuhara Y. In situ electron microscopy analysis of electrochemical Zn deposition onto an electrode. *J Power Sources.* 2021;481:228831.

30. Otani T, Nagata M, Fukunaka Y, Homma T. Morphological evolution of mossy structures during the electrodeposition of zinc from an alkaline zincate solution. *Electrochim Acta.* 2016;206:366-373.

31. Biton M, Tariq F, Yufit V, Chen Z, Brandon N. Integrating multi-length scale high resolution 3D imaging and modelling in the characterisation and identification of mechanical failure sites in electrochemical dendrites. *Acta Mater.* 2017;141:39-46.

32. Lu W, Zhang C, Zhang H, Li X. Anode for zinc-based batteries: challenges, strategies, and prospects. *ACS Energy Lett.* 2021;6(8):2765-2785.

33. Verma V, Kumar S, Manalastas W, Srinivasan M. Undesired reactions in aqueous rechargeable zinc ion batteries. *ACS Energy Lett.* 2021;6(5):1773-1785.

34. Zhang Z, Xi H, Ma X, et al. Recent progress, mechanisms, and perspectives for crystal and interface chemistry applying to the Zn metal anodes in aqueous zinc-ion batteries. *SusMat.* 2022;2(2):114-141.

35. Chen Y, Luo Y, Zhang H, Qu C, Zhang H, Li X. The challenge of lithium metal anodes for practical applications. *Small Methods.* 2019;3(7):1800551.

36. Wang D, Zhang W, Zheng W, Cui X, Rojo T, Zhang Q. Towards high-safe lithium metal anodes: suppressing lithium dendrites via tuning surface energy. *Adv Sci.* 2017;4(1):1600168.

37. Li C, Wang L, Zhang J, et al. Roadmap on the protective strategies of zinc anodes in aqueous electrolyte. *Energy Storage Mater.* 2022;44:104-135.

38. Wang X, Meng J, Lin X, et al. Stable zinc metal anodes with textured crystal faces and functional zinc compound coatings. *Adv Funct Mater.* 2021;31(48):2106114.

39. Yang Q, Li L, Hussain T, et al. Stabilizing interface pH by N-modified graphdiyne for dendrite-free and high-rate aqueous Zn-ion batteries. *Angew Chem Int Ed.* 2022;134(6):e202112304.

40. Xiao P, Li H, Fu J, et al. An anticorrosive zinc metal anode with ultra-long cycle life over one year. *Energy Environ Sci.* 2022;15(4):1638-1646.

41. Yang Z, Zhang Q, Xie C, et al. Electrochemical interface reconstruction to eliminate surface heterogeneity for

dendrite-free zinc anodes. _Energy Storage Mater_. 2022;47: 319-326.

42. Di S, Nie X, Ma G, et al. Zinc anode stabilized by an organic-inorganic hybrid solid electrolyte interphase. _Energy Storage Mater_. 2021;43:375-382.

43. Qiu H, Du X, Zhao J, et al. Zinc anode-compatible in-situ solid electrolyte interphase via cation solvation modulation. _Nat Commun_. 2019;10:5374.

44. Zeng X, Mao J, Hao J, et al. Electrolyte design for in situ construction of highly Zn^{2+}-conductive solid electrolyte interphase to enable high-performance aqueous Zn-ion batteries under practical conditions. _Adv Mater_. 2021; 33(11):2007416.

45. Yang H, Chang Z, Qiao Y, et al. Constructing a super-saturated electrolyte front surface for stable rechargeable aqueous zinc batteries. _Angew Chem Int Ed_. 2020;59(24):9377-9381.

46. Guo S, Qin L, Zhang T, et al. Fundamentals and perspectives of electrolyte additives for aqueous zinc-ion batteries. _Energy Storage Mater_. 2021;34:545-562.

47. Chang Z, Yang H, Qiao Y, Zhu X, He P, Zhou H. Tailoring the solvation sheath of cations by constructing electrode front-faces for rechargeable batteries. _Adv Mater_. 2022;34(34): e2201339.

48. Cao J, Zhang D, Zhang X, Zeng Z, Qin J, Huang Y. Strategies of regulating Zn^{2+} solvation structures for dendrite-free and side reaction-suppressed zinc-ion batteries. _Energy Environ Sci_. 2022;15(2):499-528.

49. Yao R, Qian L, Sui Y, et al. A versatile cation additive enabled highly reversible zinc metal anode. _Adv Energy Mater_. 2021; 12(2):2102780.

50. Li TC, Lim Y, Li XL, et al. A universal additive strategy to reshape electrolyte solvation structure toward reversible Zn storage. _Adv Energy Mater_. 2022;12(15):2103231.

51. Cao L, Li D, Hu E, et al. Solvation structure design for aqueous Zn metal batteries. _J Am Chem Soc_. 2020;142(51): 21404-21409.

52. Xie F, Li H, Wang X, et al. Mechanism for zincophilic sites on zinc-metal anode hosts in aqueous batteries. _Adv Energy Mater_. 2021;11(9):2003419.

53. Ma L, Li Q, Ying Y, et al. Toward practical high-areal-capacity aqueous zinc-metal batteries: quantifying hydrogen evolution and a solid-ion conductor for stable zinc anodes. _Adv Mater_. 2021;33(12):2007406.

54. Deng C, Xie X, Han J, et al. A sieve-functional and uniform-porous Kaolin layer toward stable zinc metal anode. _Adv Funct Mater_. 2020;30(21):2000599.

55. Zhao R, Yang Y, Liu G, et al. Redirected Zn electrodeposition by an anti-corrosion elastic constraint for highly reversible Zn anodes. _Adv Funct Mater_. 2020;31(2):2001867.

56. Xie X, Liang S, Gao J, et al. Manipulating the ion-transfer kinetics and interface stability for high-performance zinc metal anodes. _Energy Environ Sci_. 2020;13(2):503-510.

57. He H, Tong H, Song X, Song X, Liu J. Highly stable Zn metal anodes enabled by atomic layer deposited Al_2O_3 coating for aqueous zinc-ion batteries. _J Mater Chem A_. 2020;8(16): 7836-7846.

58. Han D, Wu S, Zhang S, et al. A corrosion-resistant and dendrite-free zinc metal anode in aqueous systems. _Small_. 2020;16(29):2001736.

59. Wang Z, Huang J, Guo Z, et al. A metal-organic framework host for highly reversible dendrite-free zinc metal anodes. _Joule_. 2019;3(5):1289-1300.

60. Liang P, Yi J, Liu X, et al. Highly reversible zn anode enabled by controllable formation of nucleation sites for Zn-based batteries. _Adv Funct Mater_. 2020;30(13):1908528.

61. Li H, Guo C, Zhang T, et al. Hierarchical confinement effect with zincophilic and spatial traps stabilized Zn-based aqueous battery. _Nano Lett_. 2022;22:4223-4231.

62. Bai Y, Zhang H, Usman Tahir M, Xiang B. Conductive copper glue constructs a reversible and stable zinc metal anode interface for advanced aqueous zinc ion battery. _J Colloid Interface Sci_. 2022;608:22-29.

63. Zhao J, Zhang J, Yang W, et al. "Water-in-deep eutectic solvent" electrolytes enable zinc metal anodes for rechargeable aqueous batteries. _Nano Energy_. 2019;57:625-634.

64. Wang D, Li Q, Zhao Y, et al. Insight on organic molecules in aqueous Zn-ion batteries with an emphasis on the Zn anode regulation. _Adv Energy Mater_. 2022;12(9):2102707.

65. Pei A, Zheng G, Shi F, Li Y, Cui Y. Nanoscale nucleation and growth of electrodeposited lithium metal. _Nano Lett_. 2017; 17(2):1132-1139.

66. Scharifker B, Hills G. Theoretical and experimental studies of multiple nucleation. _Electrochim Acta_. 1983;28(7):879-889.

67. Zhao Z, Zhao J, Hu Z, et al. Long-life and deeply recharge-able aqueous Zn anodes enabled by a multifunctional brightener-inspired interphase. _Energy Environ Sci_. 2019; 12(6):1938-1949.

68. Yang J-M, Hsieh Y-T, Chu-Tien T-T, Sun IW. Electrodeposition of distinct one-dimensional Zn biaxial microbelt from the zinc chloride-1-ethyl-3-methylidazolium chloride ionic liquid. _J Electrochem Soc_. 2011;158(5):D235.

69. Foroozan T, Yurkiv V, Sharifi-Asl S, Rojaee R, Mashayek F, Shahbazian-Yassar R. Non-dendritic Zn electrodeposition enabled by zincophilic graphene substrates. _ACS Appl Mater Interfaces_. 2019;11(47):44077-44089.

70. Li S, Fu J, Miao G, et al. Toward planar and dendrite-free Zn electrodepositions by regulating Sn-crystal textured surface. _Adv Mater_. 2021;33(21):2008424.

71. Yan Y, Shu C, Zeng T, et al. Surface-preferred crystal plane growth enabled by underpotential deposited monolayer toward dendrite-free zinc anode. _ACS Nano_. 2022;16(6):9150-9162.

72. Zheng J, Yin J, Zhang D, et al. Spontaneous and field-induced crystallographic reorientation of metal electrodeposits at battery anodes. _Sci Adv_. 2020;6(25):eabb1122.

73. Isaev V, Grishenkova O. Kinetics of electrochemical nucleation and growth. _Electrochem Commun_. 2001;3(9):500-504.

74. Gunawardena G, Hills G, Montenegro I, Scharifker B. Electrochemical nucleation: part I. general considerations. _J Electroanal Chem Interfacial Electrochem_. 1982;138(2): 225-239.

75. Scharifker BR, Mostany J. Three-dimensional nucleation with diffusion controlled growth: part I. Number density of active sites and nucleation rates per site. _J Electroanal Chem Interfacial Electrochem_. 1984;177(1-2):13-23.

76. Hariprakash B, Martha SK, Jaikumar A, Shukla AK. On-line monitoring of lead–acid batteries by galvanostatic non-destructive technique. _J Power Sources_. 2004;137(1): 128-133.

77. Subramanian VR, Boovaragavan V, Ramadesigan V, Arabandi M. Mathematical model reformulation for lithium-ion battery simulations: galvanostatic boundary conditions. *J Electrochem Soc.* 2009;156(4):A260.

78. Jilte R, Kumar R. Numerical investigation on cooling performance of Li-ion battery thermal management system at high galvanostatic discharge. *Eng Sci Technol.* 2018;21(5):957-969.

79. Lu B, Song Y, Zhang J. Selection of charge methods for lithium ion batteries by considering diffusion induced stress and charge time. *J Power Sources.* 2016;320:104-110.

80. Yuan Y, Luo G, Li N. New in situ description of electrodepositing multiple nucleation processes under galvanostatic stimuli. *RSC Adv.* 2021;11(50):31526-31532.

81. Hao J, Li X, Zeng X, Li D, Mao J, Guo Z. Deeply understanding the Zn anode behaviour and corresponding improvement strategies in different aqueous Zn-based batteries. *Energy Environ Sci.* 2020;13(11):3917-3949.

82. Li Q, Zhao Y, Mo F, et al. Dendrites issues and advances in Zn anode for aqueous rechargeable Zn-based batteries. *EcoMat.* 2020;2(3):e12035.

83. Cao Q, Gao H, Gao Y, et al. Regulating dendrite-free zinc deposition by 3D zincopilic nitrogen-doped vertical graphene for high-performance flexible Zn-ion batteries. *Adv Funct Mater.* 2021;31(37):2103922.

84. Chen T, Wang Y, Yang Y, et al. Heterometallic seed-mediated zinc deposition on inkjet printed silver nanoparticles toward foldable and heat-resistant zinc batteries. *Adv Funct Mater.* 2021;31(24):2101607.

85. Zhang Q, Luan J, Huang X, et al. Simultaneously regulating the ion distribution and electric field to achieve dendrite-free zn anode. *Small.* 2020;16(35):2000929.

86. Xie S, Li Y, Li X, et al. Stable zinc anodes enabled by zincophilic Cu nanowire networks. *Nano-Micro Lett.* 2022;14:39.

87. Yu H, Zeng Y, Li NW, Luan D, Yu L, Lou X. Confining Sn nanoparticles in interconnected N-doped hollow carbon spheres as hierarchical zincophilic fibers for dendrite-free Zn metal anodes. *Sci Adv.* 2022;8(10):eabm5766.

88. Xue P, Guo C, Wang N, et al. Synergistic manipulation of Zn^{2+} ion flux and nucleation induction effect enabled by 3D hollow SiO_2/TiO_2/carbon fiber for long-lifespan and dendrite-free Zn–metal composite anodes. *Adv Funct Mater.* 2021;31(50):2106417.

89. Pu X, Jiang B, Wang X, et al. High-performance aqueous zinc-ion batteries realized by MOF materials. *Nano-Micro Lett.* 2020;121:152.

90. Zheng J, Zhao Q, Tang T, et al. Reversible epitaxial electrodeposition of metals in battery anodes. *Science.* 2019;366(6465):645-648.

91. Pu SD, Gong C, Tang YT, et al. Achieving ultra-high rate planar and dendrite-free zinc electroplating for aqueous zinc battery anodes. *Adv Mater.* 2022;34:2202552.

92. Chu M, McBreen J, Adzig G. Substrate effects on zinc deposition from zincate solutions: I. Deposition on Cu, Au, Cd and Zn. *J Electrochem Soc.* 1981;128(11):2281-2286.

93. McBreen J, Chu M, Adzic G. Substrate effects on zinc deposition from zincate solutions: II. Deposition on Pb, Tl, Sn, and In. *J Electrochem Soc.* 1981;128(11):2287-2292.

94. Zheng J, Deng Y, Yin J, et al. Textured electrodes: manipulating built-in crystallographic heterogeneity of metal electrodes via severe plastic deformation. *Adv Mater.* 2022;34(1):2106867.

95. Zhou M, Guo S, Li J, et al. Surface-preferred crystal plane for a stable and reversible zinc anode. *Adv Mater.* 2021;33(21):2100187.

96. Li M, Ran L, Knibbe R. Zn electrodeposition by an in situ electrochemical liquid phase transmission electron microscope. *J Phys Chem Lett.* 2021;12(2):913-918.

97. Cai Z, Wang J, Lu Z, et al. Ultrafast metal electrodeposition revealed by in situ optical imaging and theoretical modeling towards fast-charging Zn battery chemistry. *Angew Chem Int Ed.* 2022;134(14):e202116560.

98. Zhang Z, Zhou X, Liu Z. Optimization of lithium nucleation by current density toward dendrite-free Li metal anode. *J Alloys Compd.* 2022;893:162389.

99. Youssef KM, Koch CC, Fedkiw PS. Influence of pulse plating parameters on the synthesis and preferred orientation of nanocrystalline zinc from zinc sulfate electrolytes. *Electrochim Acta.* 2008;54(2):677-683.

100. Garcia G, Ventosa E, Schuhmann W. Complete prevention of dendrite formation in Zn metal anodes by means of pulsed charging protocols. *ACS Appl Mater Interfaces.* 2017;9(22):18691-18698.

101. Silva Filho JF, Lins VFC. Crystallographic texture and morphology of an electrodeposited zinc layer. *Surf Coat Technol.* 2006;200(9):2892-2899.

102. Ma L, Schroeder MA, Borodin O. et al. Realizing high zinc reversibility in rechargeable batteries. *Nat Energy.* 2020;5(10):743-749.

103. Bai P, Li J, Brushett FR, Bazant MZ. Transition of lithium growth mechanisms in liquid electrolytes. *Energy Environ Sci.* 2016;9(10):3221-3229.

104. Liu Y, Xu X, Sadd M, et al. Insight into the critical role of exchange current density on electrodeposition behavior of lithium metal. *Adv Sci.* 2021;8(5):2003301.

105. Hou Z, Gao Y, Zhou R, Zhang B. Unraveling the rate-dependent stability of metal anodes and its implication in designing cycling protocol. *Adv Funct Mater.* 2021;32(7):2107584.

106. Liu H, Zhang Y, Wang C, Glazer JN, Shan Z, Liu N. Understanding and controlling the nucleation and growth of zn electrodeposits for aqueous zinc-ion batteries. *ACS Appl Mater Interfaces.* 2021;13(28):32930-32936.

107. Glatz H, Tervoort E, Kundu D. Unveiling critical insight into the Zn metal anode cyclability in mildly acidic aqueous electrolytes: implications for aqueous zinc batteries. *ACS Appl Mater Interfaces.* 2020;12(3):3522-3530.

108. Abelha Carrijo Gonçalves G, Manoel Silveira Campos P, Costa Veloso T, Rosa Capelossi V. Influence of current density and temperature in the zinc electroplating process at sulfate-based acid solution: study on process efficiency and coating morphology. *Sci Plena.* 2021;17(10):103401.

109. Wang K, Xiao Y, Pei P, Liu X, Wang Y. A Phase-field model of dendrite growth of electrodeposited zinc. *J Electrochem Soc.* 2019;166(10):D389-D394.

110. Su J, Yin X, Zhao H, et al. Temperature-dependent nucleation and electrochemical performance of Zn metal anodes. *Nano Lett.* 2022;22(4):1549-1556.

111. Zhou J, Yuan H, Li J, et al. Highly reversible and stable Zn metal anode under wide temperature conditions enabled by modulating electrolyte chemistry. *Chem Eng J.* 2022;442: 136218.

112. Krezel A, Maret W. The biological inorganic chemistry of zinc ions. *Arch Biochem Biophys.* 2016;611:3-19.

113. Jia X, Liu C, Neale ZG, Yang J, Cao G. Active materials for aqueous zinc ion batteries: synthesis, crystal structure, morphology, and electrochemistry. *Chem Rev.* 2020;120(15):7795-7866.

114. Lee S, Kang I, Kim J, et al. Real-time visualization of Zn metal plating/stripping in aqueous batteries with high areal capacities. *J Power Sources.* 2020;472:228334.

115. Cai Z, Ou Y, Wang J, et al. Chemically resistant Cu–Zn/Zn composite anode for long cycling aqueous batteries. *Energy Storage Mater.* 2020;27:205-211.

116. Wippermann K, Schultze JW, Kessel R, Penninger J. The inhibition of zinc corrosion by bisaminotriazole and other triazole derivatives. *Corrosion Sci.* 1991;32(2):205-230.

117. Parker JF, Chervin CN, Nelson ES, Rolison DR, Long JW. Wiring zinc in three dimensions re-writes battery performance—dendrite-free cycling. *Energy Environ Sci.* 2014;7(3):1117-1124.

118. Yu W, Shang W, He Y, Zhao Z, Ma Y, Tan P. Unraveling the mechanism of non-uniform zinc deposition in rechargeable zinc-based batteries with vertical orientation. *Chem Eng J.* 2022;431:134032.

119. Hao J, Li X, Zhang S, et al. Designing dendrite-free zinc anodes for advanced aqueous zinc batteries. *Adv Funct Mater.* 2020;30(30):2001263.

120. Hao J, Li B, Li X, et al. An in-depth study of Zn metal surface chemistry for advanced aqueous Zn-ion batteries. *Adv Mater.* 2020;32(34):2003021.

121. Jo JH, Aniskevich Y, Kim J, et al. New insight on open-structured sodium vanadium oxide as high-capacity and long life cathode for Zn–ion storage: structure, electrochemistry, and first-principles calculation. *Adv Energy Mater.* 2020; 10(40):2001595.

122. Yang G, Li Q, Ma K, Honga C, Wang C. The degradation mechanism of vanadium oxide-based aqueous zinc-ion batteries. *J Mater Chem A.* 2020;8(16):8084-8095.

123. Jin S, Zhang D, Sharma A, et al. Stabilizing zinc electro-deposition in a battery anode by controlling crystal growth. *Small.* 2021;17(33):2101798.

124. Huang Y, Gu Q, Guo Z, et al. Unraveling dynamical behaviors of zinc metal electrodes in aqueous electrolytes through an operando study. *Energy Storage Mater.* 2022;46:243-251.

125. Wang L, Zhang Y, Hu H, et al. A $Zn(ClO_4)_2$ electrolyte enabling long-life zinc metal electrodes for rechargeable aqueous zinc batteries. *ACS Appl Mater Interfaces.* 2019; 11(45):42000-42005.

126. Zhang N, Cheng F, Liu Y, et al. Cation-deficient spinel $ZnMn_2O_4$ cathode in $Zn(CF_3SO_3)_2$ electrolyte for rechargeable aqueous Zn-ion battery. *J Am Chem Soc.* 2016;138(39): 12894-12901.

127. Cao L, Li D, Pollard T, et al. Fluorinated interphase enables reversible aqueous zinc battery chemistries. *Nat Nanotechnol.* 2021;16(8):902-910.

128. Deng W, Zhou Z, Li Y, et al. High-capacity layered magnesium vanadate with concentrated gel electrolyte toward high-performance and wide-temperature zinc-ion battery. *ACS Nano.* 2020;14(11):15776-15785.

129. Patil N, Cruz C, Ciurduc D, Mavrandonakis A, Palma J, Marcilla R. An ultrahigh performance zinc-organic battery using poly(catechol) cathode in $Zn(TFSI)_2$-based concentrated aqueous electrolytes. *Adv Energy Mater.* 2021;11(26):2100939.

130. Pan H, Ellis JF, Li X, Nie Z, Chang HJ, Reed D. Electrolyte effect on the electrochemical performance of mild aqueous zinc-electrolytic manganese dioxide batteries. *ACS Appl Mater Interfaces.* 2019;11(41):37524-37530.

131. Luo Y, Zheng F, Liu L, et al. A high-power aqueous zinc-organic radical battery with tunable operating voltage triggered by selected anions. *ChemSusChem.* 2020;13(9):2239-2244.

132. Xu C, Li B, Du H, Kang F. Energetic zinc ion chemistry: the rechargeable zinc ion battery. *Angew Chem Int Ed.* 2012; 124(4):957-959.

133. Kim DY, Lee CH, Jeong SK. Effect of electrolyte concentration on electrochemical properties of zinc hexacyanoferrate electrode in zinc-ion batteries. *Key Eng Mater.* 2018;773:133-137.

134. Kasiri G, Trócoli R, Bani Hashemi A, La Mantia F. An electrochemical investigation of the aging of copper hexacyanoferrate during the operation in zinc-ion batteries. *Electrochim Acta.* 2016;222:74-83.

135. Yuan D, Zhao J, Ren H, et al. Anion texturing towards dendrite-free Zn anode for aqueous rechargeable batteries. *Angew Chem Int Ed.* 2021;133(13):7289-7295.

136. Hoang TKA, Acton M, Chen HTH, Huang Y, Doan TNL, Chen P. Sustainable gel electrolyte containing Pb^{2+} as corrosion inhibitor and dendrite suppressor for the zinc anode in the rechargeable hybrid aqueous battery. *Mater Today Energy.* 2017;4:34-40.

137. Cao J, Zhang D, Yue Y, et al. Regulating solvation structure to stabilize zinc anode by fastening the free water molecules with an inorganic colloidal electrolyte. *Nano Energy.* 2022;93: 106839.

138. Li Y, Wu P, Zhong W, et al. A progressive nucleation mechanism enables stable zinc stripping–plating behavior. *Energy Environ Sci.* 2021;14(10):5563-5571.

139. Chang G, Liu S, Fu Y, et al. Inhibition role of trace metal ion additives on zinc dendrites during plating and striping processes. *Adv Mater Interfaces.* 2019;6(23):1901358.

140. Olbasa BW, Huang CJ, Fenta FW, et al. Highly reversible Zn metal anode stabilized by dense and anion-derived passivation layer obtained from concentrated hybrid aqueous electrolyte. *Adv Funct Mater.* 2021;32(7):2103959.

141. Sun KEK, Hoang TKA, Doan TNL, Yu Y, Chen P. Highly sustainable zinc anodes for a rechargeable hybrid aqueous battery. *Chemistry.* 2018;24(7):1667-1673.

142. Jin Y, Zou L, Liu L, et al. Joint charge storage for high-rate aqueous zinc–manganese dioxide batteries. *Adv Mater.* 2019;31(29):1900567.

143. Park JH, Schneider NM, Steingart DA, Deligianni H, Kodambaka S, Ross FM. Control of growth front evolution by Bi additives during ZnAu electrodeposition. *Nano Lett.* 2018;18(2):1093-1098.

144. Lee S-M, Kim Y-J, Eom S-W, Choi NS, Kim KW, Cho SB. Improvement in self-discharge of Zn anode by applying surface modification for Zn-air batteries with high energy density. *J Power Sources.* 2013;227:177-184.

145. Du Y, Li Y, Xu BB, et al. Electrolyte salts and additives regulation enables high performance aqueous zinc ion batteries: a mini review. *Small*. 2021:2104640.

146. Zhang X, Hu JP, Fu N, et al. Comprehensive review on zinc-ion battery anode: challenges and strategies. *InfoMat*. 2022;4:e12306.

147. Wan F, Zhang L, Dai X, Wang X, Niu Z, Chen J. Aqueous rechargeable zinc/sodium vanadate batteries with enhanced performance from simultaneous insertion of dual carriers. *Nat Commun*. 2018;9:1656.

148. Guo X, Zhang Z, Li J, et al. Alleviation of dendrite formation on zinc anodes via electrolyte additives. *ACS Energy Lett*. 2021;6(2):395-403.

149. Otani T, Fukunaka Y, Homma T. Effect of lead and tin additives on surface morphology evolution of electrodeposited zinc. *Electrochim Acta*. 2017;242:364-372.

150. Kryshtop Y, Yurchenko N, Trofimenko V. Inhibition of galvanostatic nucleation of zinc from a zincate solution by cations of the polymeric tetraalkylammonium salt. *ECS Trans*. 2007;6(8):165-177.

151. Ma L, Pollard TP, Zhang Y, et al. Functionalized phosphonium cations enable zinc metal reversibility in aqueous electrolytes. *Angew Chem Int Ed*. 2021;133(22):12546-12553.

152. Han SD, Rajput NN, Qu X, et al. Origin of electrochemical, structural, and transport properties in nonaqueous zinc electrolytes. *ACS Appl Mater Interfaces*. 2016;8(5):3021-3031.

153. Mouanga M, Ricq L, Douglade G, Douglade J, Berçot P. Influence of coumarin on zinc electrodeposition. *Surf Coat Technol*. 2006;201(3-4):762-767.

154. Li C, Shyamsunder A, Hoane AG, et al. Highly reversible Zn anode with a practical areal capacity enabled by a sustainable electrolyte and superacid interfacial chemistry. *Joule*. 2022;6(5):1103-1120.

155. Hu C-C, Chang C-Y. Anodic stripping of zinc deposits for aqueous batteries: effects of anions, additives, current densities, and plating modes. *Mater Chem Phys*. 2004;86(1):195-203.

156. Banik SJ, Akolkar R. Suppressing dendrite growth during zinc electrodeposition by PEG-200 additive. *J Electrochem Soc*. 2013;160(11):D519-D523.

157. Youssef KMS, Koch CC, Fedkiw PS. Influence of additives and pulse electrodeposition parameters on production of nano-crystalline zinc from zinc chloride electrolytes. *J Electrochem Soc*. 2004;151(2):C103.

158. Nayana KO, Venkatesha TV. Synergistic effects of additives on morphology, texture and discharge mechanism of zinc during electrodeposition. *J Electroanal Chem*. 2011;663(2):98-107.

159. Bani Hashemi A, Kasiri G, La Mantia F. The effect of polyethyleneimine as an electrolyte additive on zinc electrodeposition mechanism in aqueous zinc-ion batteries. *Electrochim Acta*. 2017;258:703-708.

160. Guan K, Tao L, Yang R, et al. Anti-corrosion for reversible zinc anode via a hydrophobic interface in aqueous zinc batteries. *Adv Energy Mater*. 2022;12(9):2103557.

161. Sun KE, Hoang TK, Doan TN, et al. Suppression of dendrite formation and corrosion on zinc anode of secondary aqueous batteries. *ACS Appl Mater Interfaces*. 2017;9(11):9681-9687.

162. Bayaguud A, Luo X, Fu Y, Zhu C. Cationic surfactant-type electrolyte additive enables three-dimensional dendrite-free zinc anode for stable zinc-ion batteries. *ACS Energy Lett*. 2020;5(9):3012-3020.

163. Hao J, Long J, Li B, et al. Toward high-performance hybrid Zn-based batteries via deeply understanding their mechanism and using electrolyte additive. *Adv Funct Mater*. 2019;29(34):1903605.

164. Lu H, Zhang X, Luo M, et al. Amino acid-induced interface charge engineering enables highly reversible Zn anode. *Adv Funct Mater*. 2021;31(45):2103514.

165. Huang C, Zhao X, Liu S, et al. Stabilizing zinc anodes by regulating the electrical double layer with saccharin anions. *Adv Mater*. 2021;33(38):2100445.

166. Sun P, Ma L, Zhou W, et al. Simultaneous regulation on solvation shell and electrode interface for dendrite-free Zn ion batteries achieved by a low-cost glucose additive. *Angew Chem Int Ed*. 2021;133(33):18395-18403.

167. Zhang Q, Ma Y, Lu Y, et al. Designing anion-type water-free Zn^{2+} solvation structure for robust Zn metal anode. *Angew Chem Int Ed*. 2021;133(43):23545-23552.

168. Mitha A, Yazdi AZ, Ahmed M, Chen P. Surface adsorption of polyethylene glycol to suppress dendrite formation on zinc anodes in rechargeable aqueous batteries. *ChemElectroChem*. 2018;5(17):2409-2418.

169. Nian Q, Wang J, Liu S, et al. Aqueous batteries operated at −50 degrees C. *Angew Chem Int Ed*. 2019;58(47):16994-16999.

170. Kao-ian W, Nguyen MT, Yonezawa T, et al. Highly stable rechargeable zinc-ion battery using dimethyl sulfoxide electrolyte. *Mater Today Energy*. 2021;21:100738.

171. Hou Z, Tan H, Gao Y, Li M, Lu Z, Zhang B. Tailoring desolvation kinetics enables stable zinc metal anodes. *J Mater Chem A*. 2020;8(37):19367-19374.

172. Zhao X, Zhang X, Dong N, et al. Advanced buffering acidic aqueous electrolytes for ultra-long life aqueous zinc-ion batteries. *Small*. 2022;18(21):2200742.

173. Huang J, Chi X, Han Q, et al. Thickening and homogenizing aqueous electrolyte towards highly efficient and stable Zn metal batteries. *J Electrochem Soc*. 2019;166(6):A1211-A1216.

174. Feng D, Cao F, Hou L, Li T, Jiao Y, Wu P. Immunizing aqueous Zn batteries against dendrite formation and side reactions at various temperatures via electrolyte additives. *Small*. 2021;17(42):2103195.

175. Hao J, Yuan L, Ye C, et al. Boosting zinc electrode reversibility in aqueous electrolytes by using low-cost antisolvents. *Angew Chem Int Ed*. 2021;60(13):7366-7375.

176. Miao L, Wang R, Di S, et al. Aqueous electrolytes with hydrophobic organic cosolvents for stabilizing zinc metal anodes. *ACS Nano*. 2022;16(6):9667-9678.

177. Dong Y, Miao L, Ma G, et al. Non-concentrated aqueous electrolytes with organic solvent additives for stable zinc batteries. *Chem Sci*. 2021;12(16):5843-5852.

178. Chang N, Li T, Li R, et al. An aqueous hybrid electrolyte for low-temperature zinc-based energy storage devices. *Energy Environ Sci*. 2020;13(10):3527-3535.

179. Xu W, Zhao K, Huo W, et al. Diethyl ether as self-healing electrolyte additive enabled long-life rechargeable aqueous zinc ion batteries. *Nano Energy*. 2019;62:275-281.

180. Han D, Wang Z, Lu H, et al. A self-regulated interface toward highly reversible aqueous zinc batteries. *Adv Energy Mater*. 2022;12(9):2102982.

181. Qiu M, Sun P, Qin A, Cui G, Mai W. Metal-coordination chemistry guiding preferred crystallographic orientation for reversible zinc anode. *Energy Storage Mater*. 2022;49: 463-470.

182. Zhao K, Liu F, Fan G, et al. Stabilizing zinc electrodes with a vanillin additive in mild aqueous electrolytes. *ACS Appl Mater Interfaces*. 2021;13(40):47650-47658.

183. Ye Z, Cao Z, Lam Chee MO, et al. Advances in Zn-ion batteries via regulating liquid electrolyte. *Energy Storage Mater*. 2020;32:290-305.

184. Li L, Liu S, Liu W, et al. Electrolyte concentration regulation boosting zinc storage stability of high-capacity $K_{0.486}V_2O_5$ cathode for bendable quasi-solid-state zinc ion batteries. *Nano-Micro Lett*. 2021;13:34.

185. Poyraz AS, Laughlin J, Zec Z. Improving the cycle life of cryptomelane type manganese dioxides in aqueous recharge-able zinc ion batteries: the effect of electrolyte concentration. *Electrochim Acta*. 2019;305:423-432.

186. Wang S, Wang Z, Yin Y, et al. A highly reversible zinc deposition for flow batteries regulated by critical concentra-tion induced nucleation. *Energy Environ Sci*. 2021;14(7): 4077-4084.

187. Wang F, Borodin O, Gao T, et al. Highly reversible zinc metal anode for aqueous batteries. *Nat Mater*. 2018;17(6): 543-549.

188. Chen CY, Matsumoto K, Kubota K, Hagiwara R, Xu Q. A room-temperature molten hydrate electrolyte for recharge-able zinc–air batteries. *Adv Energy Mater*. 2019;9(22): 1900196.

189. Wang Y, Meng X, Sun J, Liu Y, Hou L. Recent progress in "water-in-salt" electrolytes toward non-lithium based rechargeable batteries. *Front Chem*. 2020;8:595.

190. Zhu Y, Yin J, Zheng X, et al. Concentrated dual-cation electrolyte strategy for aqueous zinc-ion batteries. *Energy Environ Sci*. 2021;14(8):4463-4473.

191. Wang L, Yan S, Quilty CD, et al. Achieving stable molybdenum oxide cathodes for aqueous zinc-ion batteries in water-in-salt electrolyte. *Adv Mater Interfaces*. 2021;8(9): 2002080.

AUTHOR BIOGRAPHIES

Zixuan Li is now studying for a DPhil (PhD) in materials science at the Univer-sity of Oxford, where she is studying zinc metal anode failure mechanisms in rechargeable aqueous zinc batteries. Before that, she attained her bachelor's degree in Measurement & Control Technology and Instruments from Chongqing University in 2018 and then obtained her master's degree in Microelectronics and Solid State Electronics from Peking University in 2021, where she studied cathode materials for zinc batteries. Her research interests are the zinc-ion battery and electron microscopy.

Alex W. Robertson is a Royal Society University Research Fellow and an assist-ant professor at the University of Warwick's Department of Physics, where he studies novel functional and energy materials by transmission electron microscopy, with a particular focus on in situ and operando techniques. He attained his PhD at the University of Oxford in 2013, where he researched the chemical vapor deposition growth of graphene. He has performed research into the atomic defects of 2D materials, nanomaterial electro-catalysts, and battery anode degradation.